END

		1.0	⠠⠆45	2.8	2.5
			⠠⠆50	3.2	2.2
			⠠⠆56	3.6	
			⠑⠑⠑	4.0	2.0
		1.1			
					1.8
		1.25		1.4	1.6

MICROCOPY RESOLUTION TEST CHART

⠠⠆⠙⠁⠗⠙⠎ ⠁ ⠨⠁⠗⠙⠎ ⠎⠄⠄⠇⠂⠄⠄⠄⠄ ⠨⠁⠗⠙⠎ ⠁ ⠨⠁⠗⠙⠎ ⠁ ⠨⠁⠗⠙⠎ ⠁ ⠎⠊⠁⠗⠙⠎ ⠁ ⠎⠊⠁⠗⠙⠎ ⠁ ⠎⠊⠁⠗⠙⠎⠄⠄⠄⠄⠄⠄ ⠄⠄⠄⠄⠄ ⠄⠄ ⠄ ⠙ARDS-1963-A

AD-A157 820

RESEARCH ON THE CRYSTAL GROWTH AND DIELECTRIC PROPERTIES OF HIGH PERMITTIVITY FERROELECTRIC MATERIALS

ANNUAL REPORT FOR THE PERIOD
March 1, 1984 through February 28, 1985

CONTRACT NO. N00014-81-C-0463
PROJECT NO. NR 032-609(471)

Prepared for

Office of Naval Research
800 North Quincy Street
Arlington, VA 22217

R.R. Neurgaonkar
Program Manager

JULY 1985

Rockwell International
Science Center

DTIC FILE COPY

85   8 02   095

REPORT DOCUMENTATION PAGE

1a. REPORT SECURITY CLASSIFICATION	1b. RESTRICTIVE MARKINGS
Unclassified	

2a. SECURITY CLASSIFICATION AUTHORITY	3. DISTRIBUTION/AVAILABILITY OF REPORT
2b. DECLASSIFICATION/DOWNGRADING SCHEDULE	Approved for public release; distribution unlimited.

4. PERFORMING ORGANIZATION REPORT NUMBER(S)	5. MONITORING ORGANIZATION REPORT NUMBER(S)
SC5345.5AR	

6a. NAME OF PERFORMING ORGANIZATION	6b. OFFICE SYMBOL (If applicable)	7a. NAME OF MONITORING ORGANIZATION
Rockwell International Science Center		

6c. ADDRESS (City, State and ZIP Code)	7b. ADDRESS (City, State and ZIP Code)
1049 Camino Dos Rios Thousand Oaks, CA 91360	

8a. NAME OF FUNDING/SPONSORING ORGANIZATION	8b. OFFICE SYMBOL (If applicable)	9. PROCUREMENT INSTRUMENT IDENTIFICATION NUMBER
Office of Naval Research		Contract No. N00014-81-C-0463

8c. ADDRESS (City, State and ZIP Code)	10. SOURCE OF FUNDING NOS			
800 North Quincy Street Arlington, VA 22217	PROGRAM ELEMENT NO.	PROJECT NO.	TASK NO	WORK UNIT NO
		NR 032-609 (471)		

11. TITLE (Include Security Classification) ~~RESEARCH ON MILLIMETER WAVE DIELECTRIC MATERIALS~~ See Cover

12. PERSONAL AUTHOR(S)
Oliver, J.R.

13a. TYPE OF REPORT	13b. TIME COVERED		14. DATE OF REPORT (Yr., Mo., Day)	15. PAGE COUNT
Annual Report	FROM 03/01/84	TO 02/28/85	JULY 1985	63

16. SUPPLEMENTARY NOTATION

17	COSATI CODES		18. SUBJECT TERMS (Continue on reverse if necessary and identify by block number)
FIELD	GROUP	SUB. GR.	
			.0000005

19. ABSTRACT (Continue on reverse if necessary and identify by block number)

Millimeter wave measurements on tungsten bronze $Sr_{0.6}Ba_{0.4}Nb_2O_6$ (SBN:60) and $Ba_{2-x}Sr_xK_{1-y}Na_yNb_5O_{15}$ (BSKNN) have shown a strong temperature dependence for permittivity and dielectric loss, with both decreasing at low temperature down to 77K for the electric field parallel to the polar axis. The observed changes in and perpendicular to the polar axis are much less, being only 30-40%. A temperature sensitive peak in the polar has been observed for some samples.

First experimental determination of the millimeter wave dn/dE for SBN:60 single crystal has been demonstrated successfully at cryogenic temperature. These results are encouraging both for basic understanding of the mechanisms controlling millimeter wave susceptibilities in ferroelectric tungsten bronze as well as for practical device applications. It has been shown for SBN:60 that the large millimeter wave nonlinear response is retained at cryogenic temperature ($dn_3/dE_3 = 6 \times 10^{-7}$ m/V at 77K) while the absorption is reduced by an order of magnitude. The experimental database has allowed, for the first time, the construction of a modeling work based on coupling of the microwave field to acoustic phonons which is consistent with the observations.

20. DISTRIBUTION/AVAILABILITY OF ABSTRACT	21. ABSTRACT SECURITY CLASSIFICATION
UNCLASSIFIED/UNLIMITED ☐ SAME AS RPT. ☒ DTIC USERS ☐	Unclassified

22a. NAME OF RESPONSIBLE INDIVIDUAL	22b. TELEPHONE NUMBER (Include Area Code)	22c. OFFICE SYMBOL
R.C. Pohanka		

DD FORM 1473, 83 APR   EDITION OF 1 JAN 73 IS OBSOLETE.

SC5345.5AR

TABLE OF CONTENTS

A-1

LIST OF FIGURES

Rockwell International
Science Center

SC5345.5AR

LIST OF TABLES

1.0   INTRODUCTION AND PROGRESS SUMMARY

High permittivity ferroelectric materials such as the tungsten bronzes and perovskites have shown substantial promise for the manipulation and control of electromagnetic propagation properties at frequencies from dc to the infrared. In the last few years, interest has grown in millimeter wave applications for communications and radars, and a need has developed to characterize the linear and nonlinear dielectric properties of ferroelectrics in this new frequency range.

The research effort reported herein is part of a long-range program whose objective is to determine the range of dielectric properties attainable at millimeter wave frequencies in various classes of high permittivity ferro-electrics, and to relate these properties to fundamental crystal character-istics. This work involves the preparation of new ferroelectrics in single crystal and ceramic form, characterization of their crystal structure and low frequency dielectric response, and measurement of both linear and nonlinear dielectric properties at millimeter wave frequencies.

Much of the early effort in this program was devoted to single crys-tal strontium barium niobate (SBN), a tungsten bronze with an unusually large room-temperature dielectric response. More recently, other tungsten bronzes such as potassium lithium niobate (KLN) and barium strontium potassium sodium niobate (BSKNN) have been prepared and studied to elucidate the role of unfilled crystallographic sites in influencing dielectric loss. Currently, we are developing preparation techniques for an unusual bronze, lead barium niobate (PBN), which should exhibit exceptionally large nonlinear electrical and optical response for a Pb:Ba ratio of 60:40, where it undergoes a transi-tion from tetragonal to orthorhombic form.

During the past year, substantial progress was made in materials development and in millimeter wave characterization efforts. They included:

1. Successful growth of very large size high quality single crystal SBN:60 (2.5 × 2.5 cm) suitable for free space millimeter wave measurements.

2. Verification of the unusual millimeter wave dielectric response in SBN and BSKNN as functions of crystal orientation and temperature; extension of the measurement range up to 100 GHz and at temperatures down to 40K.

3. First experimental determination of the millimeter wave dn/dE for SBN at cryogenic temperatures.

4. Formulation of a model for millimeter wave loss in ferroelectric tungsten bronzes which is consistent with experimental observations.

These results are extremely encouraging both for basic understanding of the mechanisms controlling millimeter wave susceptibilities in ferroelectric tungsten bronzes as well as for practical device applications. We have demonstrated for SBN that a large millimeter wave nonlinear response is retained at cryogenic temperature ($dn_3/dE_3 = 5 \times 10^{-7}$ m/V at 77K) while the absorption is reduced by an order of magnitude. For the first time, the experimental database has provided sufficient evidence to allow the construction of a modeling framework based on coupling of the microwave field to acoustic phonons.

2.0 MILLIMETER WAVE APPLICATIONS

The inherent advantages of millimeter wave radar and communications systems in terms of all-weather capability compared to IR and optical sensors, and reduced weight, size and higher spatial resolution compared to conventional microwave systems, have led to increased DoD emphasis on developing short wavelength technology for a wide variety of applications. Recent advances in millimeter wave generation by solid state devices and by high power ($\sim$200 kW cw) gyrotrons have supplied additional motivation for this effort, since potential applications are no longer source technology limited.

Common requirements in all radar and communications systems include the ability to control or manipulate electromagnetic propagation properties via an active medium, and to transmit high quality beams without excessive attenuation or distortion. These requirements were recently identified at an ARO-sponsored workshop on Short Millimeter Wave Non-Reciprocal Materials and devices. It was concluded that while considerable advances have been made in the areas of sources of radiation, mixers, detectors, and receivers, there is a lack of comparable progress in the areas of components such as reciprocal and nonreciprocal devices (e.g., phase shifters, isolators and circulators) and electronic-scanning antennas. New device concepts should be explored, and better materials need to be developed (ferroelectric, ferromagnetic and semiconducting) to support these concepts.

The large nonlinear susceptibility of ferroelectric materials has the potential of a wide variety of device applications. These include electric field controlled phase shifters, phased-array antennas, dielectric lenses, switches, frequency doublers and mixers. Inherent advantages include the ability to control propagation properties by electric rather than by magnetic fields, and the potential for much higher power handling capability than comparable semiconductor devices.

These applications require development of suitable materials with low insertion loss and large nonlinear millimeter wave susceptibility. The

results presented in this report indicate that these criteria can be met in single crystal SBN at cryogenic temperatures. Advanced materials studies carried out on KLN and BSKNN indicate that their millimeter wave losses are less than those for SBN, and have potentially better overall performance characteristics.

Implementation of practical devices and systems requires the capability for producing large, high quality single crystal materials and optimizing their millimeter wave properties through composition and process control. These are the objectives of the planned effort for this year's program.

3.0 CURRENT PROGRESS

3.1 Material Development

3.1.1 Importance of Ferroelectric Family Crystals

A goal of the proposed research program is to establish classes of ferroelectric materials that are suitable for developing a better understanding of high frequency dielectric properties and that are also useful for future device studies. The following criteria have been chosen to select suitable compositions for high frequency dielectric studies:

1. Large dn/dE at low and high frequencies

2. Large electro-optic coefficient

3. Large dielectric constant

4. Low dielectric losses at high frequencies

Based on our research in the tungsten bronze and perovskite families, most of the compositions exhibit low dielectric losses with high dielectric and electro-optic coefficients at low frequencies. The systematic growth and characterization of these ferroelectric materials is an ongoing and important part of several current programs, including the present program.

Table 1 shows some of the important perovskite compositions for potential millimeter wave applications. Currently, we are developing hot-pressed dense ceramic samples of KTN and PZT/PLZT for millimeter wave evaluation using a microprocessor-controlled, oxygen atmosphere hot press. The tungsten bronze materials which have been grown and evaluated in this program are discussed in the next sections.

Table 1

Ferroelectric and Electro-Optic Data for Perovskite
Family Compositions

Composition*	T_c (°C)	Dielectric Constant	Electro-Optic Coefficient $_{51}(10^{-12}$ m/V)	dn/dE	Materials Availability
$KNbO_3$	570	1000	380	Large	Crystals & Ceramics
$KTa_{0.65}Nb_{0.35}O_3$	R.T.	8650	$r_{51} = 3000$ $r_{33} = 1400$	Large	Crystals & Ceramics
$Pb_{0.97}La_{0.02}(ZrTi)O_3$	200	1500	Large	Large	Dense Ceramics
$Pb_{0.92}La_{0.08}(Zr_{0.65}Ti_{0.35})O_3$	130	2700	Large	--	Dense Ceramics
$Pb_{0.88}La_{0.08}(Zr_{0.7}Ti_{0.3})O_3$	120	4400	Large	--	Dense Ceramics
$BaTiO_3$	127		Large	--	Crystals & Ceramics

3.1.2 Tungsten Bronze Family Compositions

The tungsten bronze family embraces some 150 known compounds and
several solid solution systems, thus offering a wide variety of ferroelectric
and paraelectric materials. However, only a few compositions have been selected
f⁻ our dielectric studies; their classification is given in Table 2.

At present, our work is heavily concentrated on three different fer-
roelectric bronze compositions, specifically SBN:60 (partially unfilled 15-
and 12-fold sites), BSKNN (15- and 12-fold sites completely filled) and KLN
(all sites completely filled); and high frequency measurements have been per-
formed from liquid nitrogen to the Curie temperature. The results are inter-
esting in that they are often quite different from one composition to another.
The information on dielectric properties obtained from these compositions has
contributed to our understanding of these materials and has indicated poten-
tial device applications.

Table 2

Ferroelectric and Electro-Optic Data for Tungsten
Bronze Family Compositions

System	T_c (°C)	Electro-Optic r_{33}	Dielectric Constant ε_{33}
SBN:60	72	420×10^{-12}	800
SBN:60:R.E.*	< 72	$> 420 \times 10^{-12}$	> 800
SBN:75	56	1400×10^{-12}	3000
PBN:60 + La^{3+}**	> 300	442×10^{-12} 750×10^{-12}	600
BSKNN	200	300×10^{-12}	< 200
KLN	405	60×10^{-12}	< 100
SNN-CNN**	~ 300	High	2800
PKN-BNN**	~ 300	High	1000
SNN-BNN**	~ 250	High	1800
$Ba_3LaNaNb_{10}O_{30}$	- 50	Large	Large
$K_2LaNb_5O_{15}$***	- 80	Large	Large

* Rare-earth doped
** Morphotropic phase boundary compositions
*** Large at low temperature

Based on our crystal chemistry work on tungsten bronze SBN:60 single crystals and ceramics, the incorporation of 3-d and 4-f ions in the lattice should be advantageous for both millimeter wave and optical device applications. Table 3 shows several proposed dopants for this work and their lattice site preferences. While the effect of these ions on optical properties is

substantial, the effect on millimeter wave dielectric losses is not yet well established; hence, examining the role of 3-d and 4-f ions to improve the millimeter wave properties at room temperature may prove worthwhile. A thorough understanding of dopant valance states, site preferences, and the effects of dopant concentration is fundamental to this work and will be explored in depth.

Table 3

Proposed Dopants for Millimeter Wave Studies in SBN

| Dopants | Valence State | Site Preference for Proposed Dopants | | | |
		15-Fold	12-Fold	9-Fold	6-Fold
Cerium	Ce^{3+}, Ce^{4+}	Ce^{3+}	Ce^{3+}	Ce^{4+}	Ce^{4+}
Terium	Tb^{3+}, Tb^{4+}	-	Tb^{3+}	Tb^{4+}	Tb^{4+}
Iron	Fe^{3+}, Fe^{2+}	-	-	Fe^{2+}	Fe^{2+}, Fe^{3+}
Manganese	Mn^{2+}, Mn^{3+}, Mn^{4+}	-	-	Mn^{2+}	Mn^{2+}, Mn^{3+}
Titanium	Ti^{4+}, Ti^{3+}	-	-	-	Ti^{4+}, Ti^{3+}
Molybdenum	Mo^{6+}, Mo^{4+}	-	-	-	Mo^{5+}, Mo^{4+}
Niobium	Nb^{5+}, Nb^{4+}	-	-	-	Nb^{5+}, Nb^{4+}

3.1.3 Single Crystal Growth of BSKNN and KLN Compositions

Both BSKNN and KLN belong to the tungsten bronze family and have a room temperature tetragonal structure with a point group 4 mm. The BSKNN crystals of the composition $Ba_{1.2}Sr_{0.8}K_{0.75}Na_{0.25}Nb_5O_{15}$ are jointly grown under Army and ONR contracts for electro-optic and millimeter wave device studies, respectively. Recently the Czochralski growth technique has undergone several modifications in order to improve overall crystal quality, particularly with regard to optical defects and striations (compositional fluctuations). Since the present BSKNN composition appears to be congruent melting, the current effort has concentrated on this composition and another

important bronze, KLN. Table 4 summarizes the growth conditions for these BSKNN and KLN crystals.

Table 4

Czochralski Growth Data for Tetragonal Tungsten Bronze Compositions

Composition	Growth Temperature (°C)	Growth Direction	Growth Habit	Crystal Diameter (cm)	Remarks
$Sr_{0.6}Ba_{0.4}Nb_2O_6$	1510	(001)	Cylindrical	~3.0	Crack-free and excellent quality
$Sr_{0.5}Ba_{0.5}Nb_2O_6$*	1500	(001)	Cylindrical	~1.8 to 2.0	Moderate quality
$Ba_{2-x}Sr_xK_{1-y}Ba_yBb_5O_{15}$	1480	(001)	Square	~0.8 to 1.0	Crack-free and good quality
$Sr_2KNb_5O_{15}$**	1480	(001)	Cylindrical	~0.5 to 0.8	Moderate quality
$K_3Li_2Nb_5O_{15}$**	1050	(001)	Square	0.3 to 0.5	Cracks
		(100)	Square	0.5 to 0.8	Crack-free, reasonable quality
		(110)	Square	0.5 to 0.8	Crack-free, reasonable quality
$K_3Li_2Nb_{5-x}Ta_xO_{15}$	1000-1250	(001) (110)	Square	0.5 to 1.0	Reasonable quality with excellent properties
$Pb_{0.33}Ba_{0.70}Nb_{1.987}O_6$***	~1350	(001)		0.8 to 1.0	Few cracks, but excellent properties

*Noncongruent melting composition
**Difficult to grow
***Grown at Penn State, difficult to grow

The Czochralski technique is now well established for these compositions, and crystals of reasonable quality and size are being produced. Figure 1 shows a typical BSKNN crystal grown along the c-axis. This crystal is a little over 1 cm in diameter, and this is the first time such large crystals of this composition have been grown. During the last year, a considerable effort was made to improve crystal quality, specifically for BSKNN, using an automatic diameter control system. The present improvements in BSKNN crystal quality and size have primarily resulted from the following changes in the growth techniques:

1. Use of higher purity starting materials to eliminate striations caused by impurity ions, e.g., Ca^{2+}, Mg^{2+}, Fe^{3+};

2. Established effective pulling and rotation rates;

3. Effectively implemented an automatic diameter control (ADC) system to minimize temperature instability during growth.

The adaption of the ADC system for BSKNN crystals is the most recent modification in this growth technology and has had a significant impact on crystal quality. Figure 2 shows striations before and after using the ADC system for this growth. ADC has also allowed us to pull crystals of uniform diameter without significant problems. In our future work, we will continue to modify this technique to obtain better quality and size crystals. The following changes are planned for future growth work:

1. Use of better starting materials to completely eliminate striations arising from impurity ions.

2. Modify the ADC system to obtain a more stable thermal environment for crystal growth.

KLN is the largest unit cell tungsten bronze grown to date (a = 12.590Å and c = 4.020Å) and is potentially interesting in comparison with the dielectric properties of SBN and other bronze compositions. Single crystal growth of KLN has been successful; however, the growth technique is confined to smaller crystals, typically 5-6 mm in diameter. The growth of this composition is extremely difficult due to the volatilization of potassium during growth, and the crystals after crack when grown along the c-axis. This cracking problem has been nearly eliminated for crystals grown along the a-axis (110) direction, and crystals as large as 5-7 mm in diameter of excellent quality have resulted. The crystals currently developed are being tested for
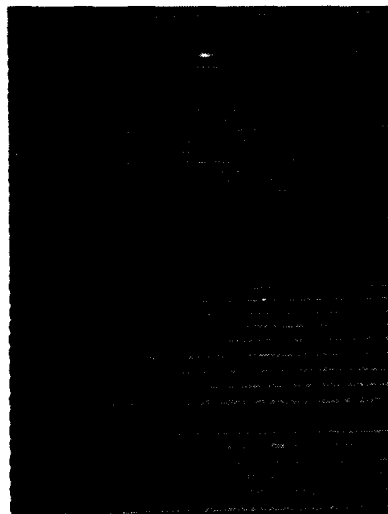
SC84-28252

Fig. 1 BSKNN single crystal grown along the c-axis.

SC84-28254

**BSKNN CRYSTAL GROWN WITHOUT
ADC SYSTEM: COMPLETELY STRIATED
CRYSTAL**

**BSKNN CRYSTAL GROWN WITH ADC
SYSTEM: STRIATIONS ALMOST
SUPPRESSED**

Fig. 2 Optical striations in Czochralski-grown BSKNN with and without
automatic diameter control (ADC).

C6986A/bw

their millimeter wave dielectric properties, and if these are found to be interesting for future studies, efforts will be made to grow crystals of larger size.

Table 5 summarizes the results of structural and ferroelectric measurements for these crystals. The temperature dependence of the dielectric constants ε_{33} and ε_{11} and dielectric loss (tan δ) were determined from (001) and (100) plates at frequencies of 1, 10, 100 and 1000 KHz. The temperature range covered was 20 to 500°C, depending upon the Curie temperature, T_c, for the given crystal. Both ε_{33} and ε_{11} showed marked anomalies at the transition point. The general temperature behavior and large anisotropy of ε_{33} and ε_{11} is typical of all the bronze crystals. However, the magnitude of the dielectric constant is markedly different for each composition and seems to depend strongly on the size of the unit cell of the given bronze crystal. For example, ε_{11} is large while ε_{33} is small for the bigger unit cell bronzes, e.g., BSKNN, KLN. On the other hand, the situation is reversed in the case of smaller unit cell bronzes, where ε_{11} is smaller and ε_{33} is larger. As summarized in Table 5, other constants such as piezoelectric and electro-optic, are also different when going from bigger to smaller unit cell bronzes.

In general, the low frequency dielectric losses for these crystals are low, on the order of 0.03 or less at room temperature, and are further reduced on cooling to liquid nitrogen or below. The low temperature/high frequency dielectric measurements are discussed in the following sections.

3.2   Millimeter Wave Measurements

The primary objectives of the millimeter wave characterization program for this year were:

1. To determine the dielectric properties of SBN and BSKNN along the principal crystal axes from 30-100 GHz as a function of temperature over the range 40-300K, to verify the anomalous temperature behavior previously observed in these materials and described in last year's annual report.

Table 5

Physical Properties of Bronze Crystals

Property	SBN:60	SBN:50	BSKNN	KLN
Lattice Constants	a = 12.462Å c = 3.938Å	a = 12.480Å c = 3.952Å	a = 12.506Å c = 3.982Å	a = 12.590Å c = 4.015Å
Curie Temperature (°C)	72°	125°C	203°C	405°C
Dielectric Constant	ε_{33} = 880	ε_{33} = 500	ε_{33} = 420	ε_{33} = 120
Electromechanical Coupling Coefficients	k_{33} = 0.47 k_{31} = 0.14 k_{15} = 0.24	k_{33} = 0.48 k_{31} = 0.137 -	k_{33} = 0.47 - k_{15} = 0.28	k_{33} = 0.52 - k_{15} = 0.36
Piezoelectric Constants C 10^{12} C/N	d_{33} = 130 d_{15} = 31	d_{33} = 100 d_{15} = 24	d_{33} = 60 d_{15} = 80	d_{33} = 57 d_{15} = 68
Electro-Optic Coefficient (M/V)	420×10^{-12}	180×10^{-12}	360×10^{-12}	60×10^{-12}

All crystals exhibit room temperature tetragonal bronze structure (4mm).

2. To determine the magnitude of the low-temperature millimeter wave nonlinear response dn/dE in SBN.

3. To initiate millimeter wave dielectric measurements on single crystal KLN ($K_3Li_2Nb_5O_{15}$), a fully "stuffed" tungsten bronze.

These tasks were performed at two separate characterization facilities, one at the Science Center and the other at the Electrical Engineering Department of UCLA under the direction of Professor Harold Fetterman. Wherever possible, the same sample, or near-identical ones prepared from adjacent locations of a given crystal boule, were used at both facilities to provide a consistency check on the results obtained. In general, different experimental methods are used. The Science Center utilizes waveguide and free-space techniques to cover the

frequency region 30-50 and 90-100 GHz. Temperature capabilities include the continuous range of 300-1700K and at discrete cryogenic fluid temperatures below 300K (77K, 87K, etc.) The UCLA facility is capable of continuous temperature coverage from 40-300K over the entire frequency range 50-110 GHz. The experimental capabilities provided by the two facilities are complementary and together represent a unique combination for experimental studies of the millimeter wave dielectric properties of materials.

For the waveguide measurements at the Science Center in the 30-50 GHz region, samples were prepared to fit the inside dimensions of a rectangular waveguide (2.845 mm × 5.69 mm). The choice of this measurement method was dictated by limitations in the sizes of single crystal ferroelectrics which can be fabricated. Up until this year's effort, dielectric measurements on advanced single crystal ferroelectrics, such as SBN and BSKNN, were carried out exclusively by this method. The complex dielectric constant of the material is then determined from the measured transmission and reflection coefficients by solving the transcendental equations for waveguide propagation through a dielectric media. In applying this to high loss/high permittivity materials, the imperfect fit of the sample in the waveguide can significantly modify the propagation, giving rise to erroneous values in the dielectric constant. Recent calculations carried out under a Science Center IR&D project indicate that this effect is quite complex and cannot be described by simple perturbation equations even for very small air gaps on the order of 1%. Theoretical models have been constructed to treat this problem, and numerical methods have been developed for its solution.

In this year's experimental effort, waveguide measurements were made with a conductive silver paint to eliminate the residual air gap, where possible. However, for the measurements of dn/dE, a gap must be present due to the requirement of conducting electrodes on the opposite edges of the sample. Consequently, the data obtained for these measurements were analyzed by the developed numerical method. As a verification, systematic studies were carried out with measurements on samples with air gaps ranging in value from 1% to 30%. The experimental results for the transmission and reflection as a function of fre-

quency were then compared with theory to determine the relative magnitudes of the dominant waveguide mode through the sample and the propagation in the air gap. These results were then used to deduce the values for dn/dE.

During the last quarter of the program, the outstanding success in the materials research portion of the program resulted in the availability of large sized, single crystal SBN samples for millimeter wave measurements. These samples are approximately 2.5 cm × 2.5 cm in size for both crystal orientations, i.e., crystal c-axis in the plane as well as perpendicular to the sample face. Such large sample sizes enabled free space measurements to be carried out at 100 GHz. These measurements are much more direct and less susceptible to systematic sources of errors. It also enabled us to measure ϵ_1 and ϵ_3 as well as dn_3/dE_3 and dn_1/dE_3 on the same sample simply by reorientation of the crystal axis with respect to the polarization direction of the incoming millimeter wave. The success in obtaining the first observation of the temperature dependence of the millimeter wave nonlinear susceptibilities are due largely to this availability of sample sizes larger than millimeter wavelengths.

In general, excellent agreement was obtained between the Science Center results and the UCLA results for the cases where the experimental conditions overlapped. Reasonable agreement was also obtained with results from previous studies in this program. The experimental method and data obtained in the study undertaken at UCLA are described separately in Section 3.2.4. Because of different approaches used in data analysis, these results are given in terms of optical constants n and k, rather than the dielectric constants, ϵ' and ϵ''. These constants are related by the expressions,

$$\epsilon' = n^2 - k^2 \quad ; \quad \epsilon'' = 2nk \quad . \tag{3.1}$$

3.2.1 Millimeter Wave Dielectric Properties of Single Crystal SBN (61/39)

The dielectric properties of single crystal SBN were measured for a number of samples at 30-50 GHz and at 90-100 GHz. These included both crystal orientations at room temperature and liquid nitrogen temperature. The results

reported are essentially all from the characterization effort performed at the
Science Center, as the current measurement technique used at UCLA is not readily
adaptable to high-loss materials. Preliminary results from the UCLA effort are
in general agreement with the results given here; and as described in Section
3.2.4, work is under way to develop a suitable capability at UCLA to enable
quantitative studies to be made on this material from 50-100 GHz at temperatures
down to 40K.

Because of the recent availability of large high quality crystal sam-
ples from the materials development effort previously described, we are able to
make the first determination of the nonlinear coefficients dn_3/dE_3 and dn_1/dE_3
at liquid nitrogen temperature. The results are extremely encouraging, as it
was demonstrated that these coefficients did not substantially decrease in value
at low temperatures. In addition, the data provided the basis for a model to
describe the fundamental mechanism controlling the susceptibility in this class
of material.

Dielectric measurements of ε', ε'' and dn_3/dE_3 were carried out using
the filled waveguide technique between 30-50 GHz on a number of samples. As we
had previously observed, there is a variation from sample to sample of the
values for ε' and ε''. The dn_3/dE_3 measurements were carried out by applying an
ac electric field across the sample and observing the resulting modulation of
the transmitted microwave power. In all cases, this modulation was found to be
linear in the applied field strength up to the maximum value of 10^6 m/V. Typi-
cal data are shown in Fig. 3 for a 1 KHz modulation frequency. The effect is
insensitive over the ac frequency range studied (0.1-10 KHz) throughout the
millimeter wave band of 30-50 GHz.

Measurements were carried out between 90-100 GHz on two plate samples
approximately 2.5 cm × 2.5 cm in size, one with the crystal c-axis in the plane
and the other with the c-axis perpendicular to the plane of the sample face.
The linear dielectric properties (ε', ε'') were then determined from the observed
microwave transmission and reflection coefficients. For the dn/dE measurements,
electrodes were deposited on opposite edges of the first sample so that the
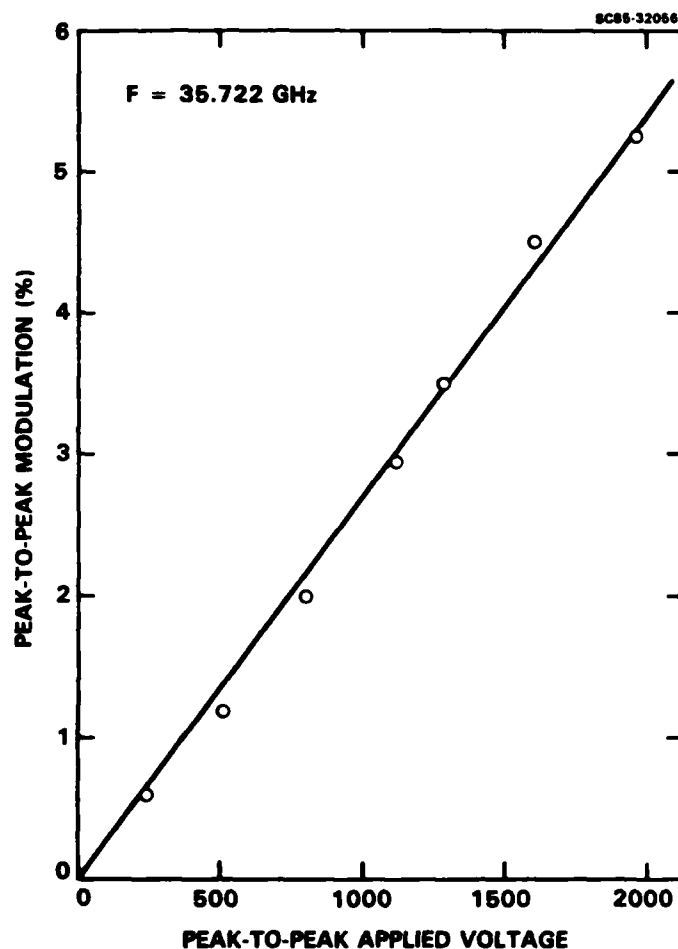
F = 35.722 GHz

SC88-32056

Fig. 3

Observed millimeter wave modulation of 1 kHz for SBN:61.

applied field is across the c-axis. By rotating the sample with respect to an incident linearly polarized microwave beam and measuring the magnitude of the modulation on the intensity of the reflected power, the coefficients dn_3/dE_3 and dn_1/dE_3 were obtained. Values for ε', ε'' and dn/dE are summarized in Table 6.

3.2.2 Millimeter Wave Dielectric Properties of Single Crystal BSKNN

The millimeter wave dielectric properties of single crystal BSKNN have been determined as a function of temperature and crystal orientation. The c-axis permittivity measurements were made from 30-100 GHz over the temperature range 40-295K. For the a-axis permittivity, measurements were made from 30-50 GHz at room temperature and at liquid nitrogen temperature, and the results are

Rockwell International
Science Center

SC5345.5AR

Table 6

Millimeter Wave Dielectric Properties of Single Crystal SBN

	Frequency (GHz)	Temperature (K)	ε'	ε''	tan δ	
c-Axis						dn_3/dE_3
Sample A	30–50	295	158	86	0.54	2.7×10^{-6}
		77	124	8.8	0.07	
Sample B	30–50	295	169	76	0.45	
Sample I	90–100	295	273	149	0.55	1.6×10^{-6}
		77	67	23	0.34	5.0×10^{-7}
c-Axis						dn_1/dE_3
Sample A	30–50	295	231	51	0.22	
		77	190	37	0.20	
Sample B	30–50	295	257	55	0.21	
Sample I	90–100	295	211	37	0.18	2.2×10^{-7}
		77	180	29	0.16	$< 5 \times 10^{-8}$
Sample II	90–100	295	216	42	0.19	

Table 7

Millimeter Wave Dielectric Properties of Single Crystal BSKNN

	Temperature (K)	ε'	ε''	tan δ
c-Axis				
Sample 1				
30-50 GHz (SC)	295	60	8.4	0.15
	77	29	1.1	0.04
50-100 GHz (UCLA)	295	53	9.5	0.18
	77	31	1.0	0.03
Sample 2				
30-50 GHz (SC)	295	48	9.2	0.19
a-Axis				
30-50 GHz (SC)	295	160	64	0.40
	77	156	56	0.36

given in Table 7. The results for the c-axis dielectric properties as a continuous function of temperature are given in Section 3.2.4.

The agreement shown for the samples characterized at the Science Center and at UCLA is excellent considering the substantial fundamental differences in the experimental techniques used. The differences in the dielectric properties reported for Samples 1 and 2 are typical of the observed variations we have found among different crystal samples for this material. The dielectric properties are insensitive to frequency throughout the range 30-100 GHz for the c-axis orientations as demonstrated by the results obtained for Sample 1.

The temperature behavior of the dielectric properties is qualitatively similar to that for SBN, i.e., a strong temperature dependence in the c-axis direction and a very weak dependence in the a-axis direction. Both the real and imaginary part of the dielectric constant remained high for the a-axis direction down to liquid nitrogen temperature. Preliminary data from the UCLA effort

indicate that this general observation holds true down to 40K. This suggests different loss mechanisms for the two crystal orientations for the tungsten bronzes in general. Identification of these mechanisms will be the objective of our continuing investigation by experimental and modeling efforts.

Recent advances in materials development have also made available samples with sizes nearly suitable for dn/dE determination using the more accurate and convenient free space measurement technique. We plan to carry out this type of measurement on BSKNN at 100-140 GHz as a function of temperature as soon as suitable samples are fabricated.

3.2.3   Millimeter Wave Dielectric Properties of Single Crystal KLN

Potassium lithium niobate ($K_3Li_2Nb_5O_{15}$) is the largest unit cell tungsten bronze successfully grown to date, and it is potentially interesting from both mechanistic and applications viewpoints. The millimeter wave characterization effort on this material is currently limited by the sizes of available samples. KLN samples have a tendency to fracture badly when grown along the crystal c-axis. Growths along the crystallographic a-axis have been successful in producing crack-free, excellent quality single crystals with diameters up to 0.7 cm. Attempts to grow crystals larger than 1 cm by the Czochralski technique have not produced fracture-free specimens to date.

Because of this fabrication difficulty, millimeter wave measurements were restricted to determination of c-axis dielectric properties at 30-50 GHz. The data obtained are summarized in Table 8.

Table 8

Room Temperature Dielectric
Properties of Single Crystal
KLN at 30-50 GHz Along the
c-Axis

ϵ'	ϵ''	tan δ
75	6.8	0.09

As can be seen, the room temperature millimeter wave loss tangent for KLN is considerably lower than that of either SBN or BSKNN. This observed trend suggests that effort be undertaken to further explore this promising material system. We are continuing this investigation to establish the temperature dependence of the dielectric constant and loss and to initiate measurements of dn/dE. Materials studies are also being pursued to fabricate samples greater than 1 cm in size.

3.2.4 Progress Summary of Effort at UCLA

The millimeter wave transmittance measurement apparatus at UCLA has now been extended to allow accurate low temperature measurements by use of a sample mounting setup shown schematically in Fig. 4. One of the waveguide flanges which contacts the sample is connected to a copper closed cycle helium refrigerator unit. The unit is inside a mechanically pumped vacuum chamber to prevent vapor condensation and heat convection. Thin polyethylene vacuum windows are placed between hollow metal waveguide sections cut approximately at the Brewster's angle for the linearly polarized TE_{10} waveguide mode to avoid extraneous standing waves. A barrier to heat conduction along the waveguides is
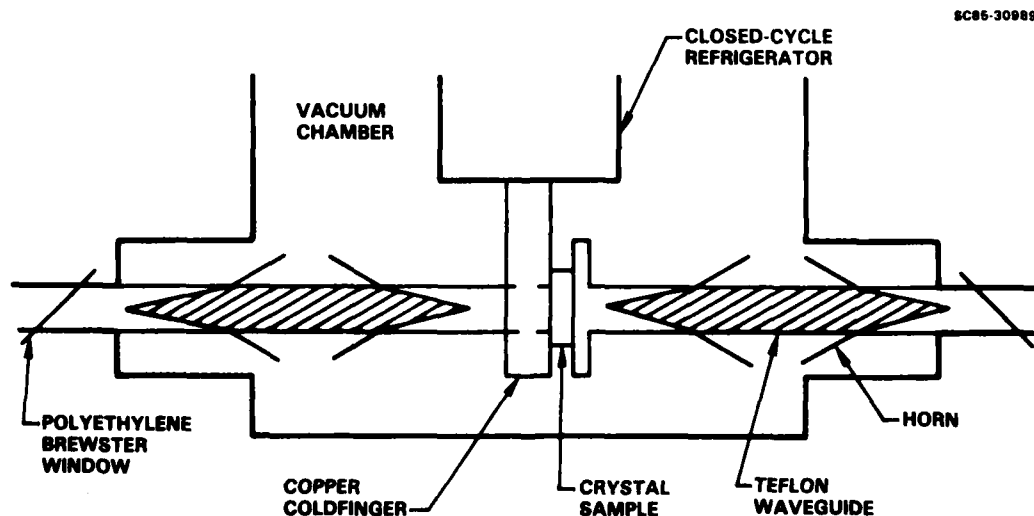
Fig. 4 Millimeter wave transmittance measurement apparatus (UCLA).

provided by solid teflon waveguide sections which slide inside the metal wave-
guide. A two-step transition is made by a pyramidal teflon taper and a metal
horn. The lowest sample temperature achievable is 40K, and a heater and diode
temperature sensor are mounted on the copper block and are connected to a com-
puter interfaced temperature controller to allow stabilization at any tempera-
ture up to 270K.

The low temperature transmittance spectrum for 60/40 SBN with the mil-
limeter wave electric field polarized perpendicular to the crystal "c" axis
shows a reduction in absorption when compared with the room temperature spec-
trum. A far greater reduction, however, is obtained for the parallel polariza-
tion. The crystal thus becomes a natural millimeter wave polarizer at low tem-
perature, transmitting one polarization much better than the other. This phe-
nomenon seems to be rather general in the tungsten bronzes. BSKNN, for example,
shows a similar effect for the parallel polarization, with close to an order of
magnitude decrease in the absorption coefficient upon cooling (Fig. 5). The
perpendicular polarization, however, does not show a significant reduction in
absorption. The smooth curve in Fig. 5 is a theoretical fit used to determine
the optical constants n and k, which are the real and negative imaginary parts
of the refractive index. This curve gives a Fabry-Perot spectrum for Fresnel
reflections from the air-dielectric interface, modified by the change in phase
velocity produced by the presence of the metal waveguide walls. The lower
absorption in BSKNN, as compared with SBN, produces Fabry-Perot fringes and
hence allows a determination of n and k all the way up to room temperature.
These optical constants are shown as functions of temperature in Figs. 6 and 7.

Figure 8 shows the loss tangent as a function of temperature. Note
that the x intercept meets the axis at the Curie temperature. Our current
analysis centers around relating this loss mechanism to the one-optic phonon
absorption by the ferroelectric soft mode. However, based upon phonon selection
rules, our models have not been able to explain the observed orientational
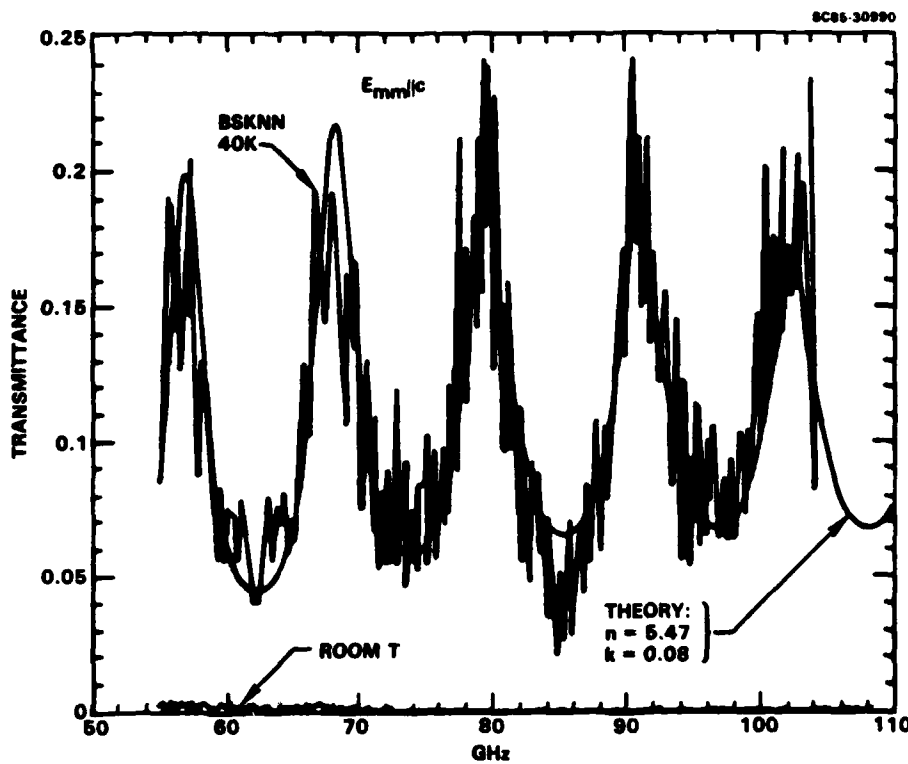dependence of absorption as a function of temperature.

Fig. 5 40K and room temperature transmittance of single crystal BSKNN
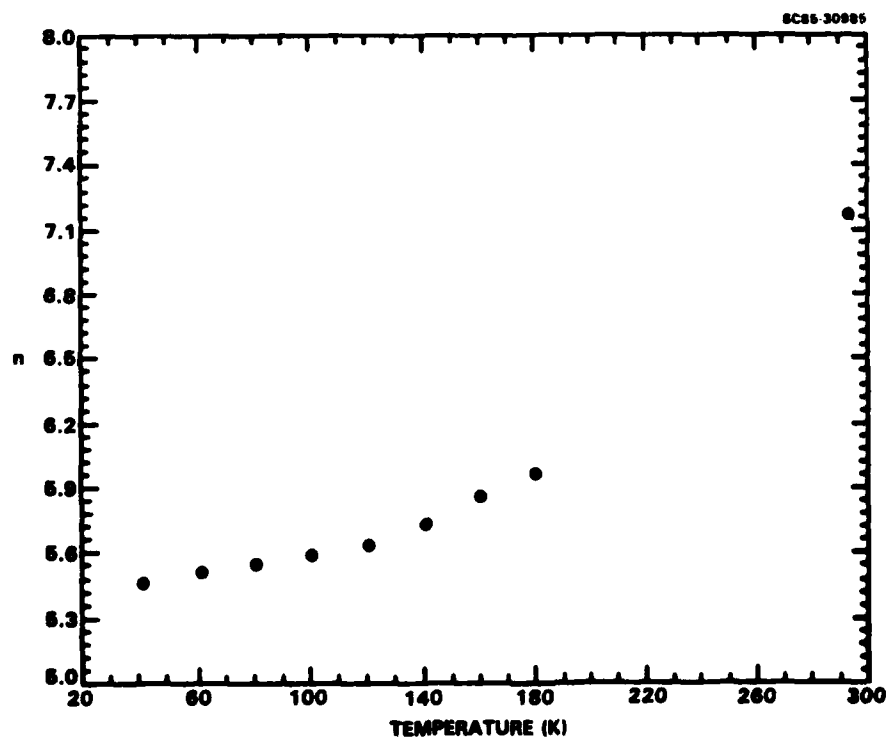for the electric field parallel to the c-axis.

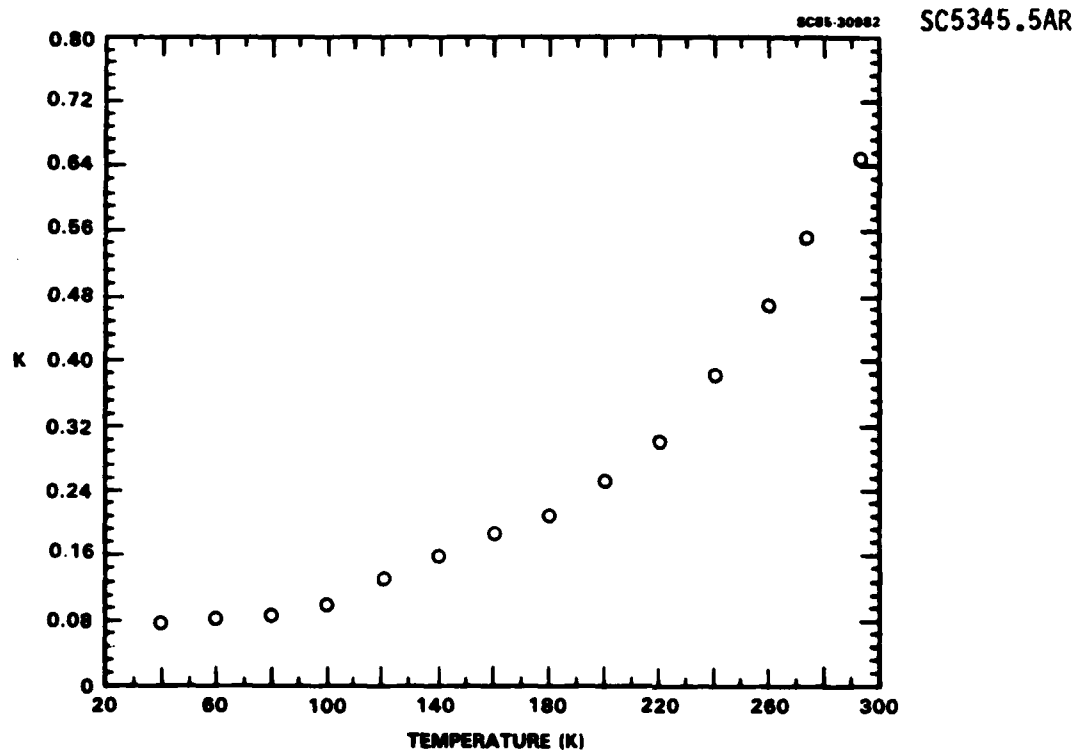Fig. 6 n vs temperature for BSKNN (50-110 GHz).

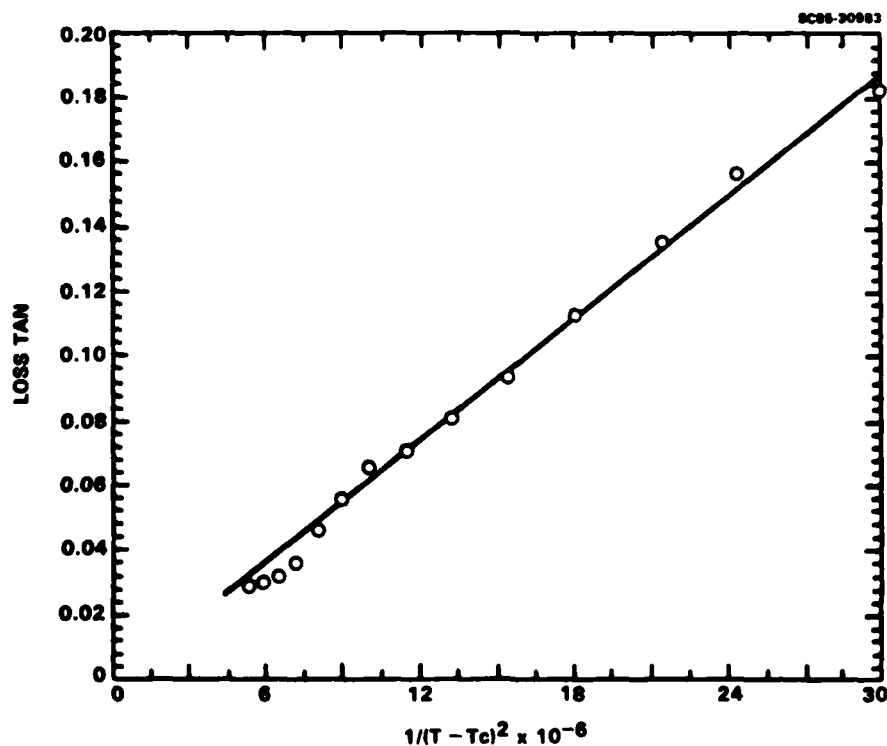Fig. 7 k vs temperature for BSKNN (50-110 GHz).

Fig. 8 Dielectric loss vs temperature for c-axis BSKNN.

The figures-of-merit must be fully considered in these measurements. For example, if we assume a (333) geometry with a parallel applied electric (E) and radiation fields, we can write for the phase retardation Γ for a path length L in the material as

$$\Gamma = \pi L n_e^2 r_{33} E / \lambda \quad , \tag{3.2}$$

where the "e" subscript identifies the extraordinary polarization direction. If L were limited by crystal availability or device geometry, the figure of merit would be

$$FOM = n_e^2 r_{33} \tag{3.3}$$

The electro-optic coefficient is expected to be a function of linear susceptibility. In general, this relationship needs to be established experimentally for individual material systems. Modeling efforts by Boyd[1] have resulted in a simple relationship $r_{33} \propto n_e^3$. For this model, the FOM = $n_e^3(n_e^2 - 1) \cong n_e^5$. Consequently, if this relationship proves to be valid, the decrease in n_e observed for SBN and BSKNN at low temperature can significantly reduce this figure-of-merit. A key requirement in the program is clearly the establishment of this temperature dependence of the electro-optic coefficient. (In single crystal SBN, preliminary data described in Section 3.2.1 have shown that the dependence in r_{33} on linear susceptibility is much slower than predicted by the n_e^5 model. This is the most encouraging data to date on potential device applications for the tungsten bronzes.)

In the case considered here, absorption is very high and limits L so that a different FOM is appropriate. In this case the loss = $1 - \exp(-4\pi k_e L/\lambda)$, where L is limited to some value inversely proportional to k_e. It is here that cooling has an important role and we must find conditions to maximize n_e^5/k_e. Cooled tungsten bronzes are thus promising candidates for use in millimeter wave electro-optic devices. This is especially apparent when one considers that the only material known to have a higher performance parameter, $BaTiO_3$, is difficult to obtain in high quality single domain crystals. The

performance of tungsten bronzes is expected to improve with continued mater-
ials research.

We have also been developing the capability to measure electro-optic
coefficients at low temperatures. Preliminary results at room temperature
have shown substantial effects at 90 GHz in several geometries. Application
of an electric field transverse to the propagation direction cannot be done
for a sample between metal waveguide flanges because the flanges divert the
field lines. We have thus made free space transverse field measurements on
samples about 1 cm from each of two waveguide horns. Quantitative analysis of
these results shows a large uncertainty in the electro-optic coefficient but
is consistent with previous measurements.

Application of a longitudinal (parallel to the propagation) electric
field is possible on a sample between metal waveguide flanges; however, the
electrodes may attenuate the power of the transmitted millimeter wave. This
problem is reduced by the use of wire polarizer electrodes, oriented perpen-
dicular to the millimeter wave polarization so that each has over 50% trans-
mittance. The change in transmittance measured was made using a fast response
diode detector input to a lock-in amplifier referenced to a 1 kHz ac voltage
applied to the crystal. Although the results were proportional to the slope
of the transmittance spectrum, they were somewhat obscured by the presence of
rapid oscillations due to the presence of extraneous standing waves.

3.3 Theoretical Modeling

Since the inception of our characterization efforts on the tungsten
bronzes, two common features of their millimeter wave dielectric properties
have resisted explanation: high losses along both crystal axes (tan $\delta \sim 0.2$);
and a major reduction in polar axis permittivity from its dc value. Stria-
tions, localized defects, and incomplete poling have all been examined and
experimentally discarded as suitable sources for this behavior.

These experimental investigations have pointed us toward the conclu-
sion that a direct coupling must exist between the microwave electric field
and lossy acoustic phonons in these systems. Such a coupling would be a

natural consequence of spatial variations in the spontaneous polarization, P_s, whatever their source.

Recently, Cross and coworkers[2] at Penn State have found evidence for a persistent, spatially varying polarization above the Curie point in SBN, with a root mean square magnitude of about one third the low-temperature P_s value. This suggests that the polarization below T_c is similarly variable.

In view of these observations, it appears worthwhile to attempt to model the effect that local variations in P_s will have on the microwave dielectric susceptibilities. As a starting point for such a model, we consider the response of an elastic continuum to an applied microwave electric field (Toupin, 1961).[3]

The equation of motion for the elastic displacement u_i in a spontaneously polarized medium takes the form

$$\rho \ddot{u}_i = \sigma_{i,k}\Big|_{E=0} - E_i \nabla \cdot P^0 - 2 \frac{\partial}{\partial x_\ell} \left(\sum Q_{jkrs} C^P_{rsi\ell} (\kappa_{jj} - 1) \epsilon_0 P^0_k E_j \right) \tag{3.4}$$

where ρ is the mass density of the medium, σ is the usual elastic stress tensor in zero electric field, E_i is the applied field, P^0 is the polarization in zero field, Q is the electrostriction tensor, C^P is the elastic constant tensor at constant pressure, κ is the dielectric tensor at the applied microwave frequency and ϵ_0 is the permittivity of vacuum. Order of magnitude estimates for a typical tungsten bronze indicate that the piezoelectric force terms (due to Q) are about a hundred times larger than the direct electric force on the equivalent charge density $\nabla \cdot P^0$.

The dielectric loss produced by the generation of damped elastic waves can be obtained to first order as the volume average of the dissipation:

$$\epsilon_0 \kappa''_i E_i^2 = \text{Im} \langle \frac{1}{V} \int F \cdot u \, d^3 r \rangle \quad . \tag{3.5}$$

Here κ_i'' is the imaginary part of h along the axis defined by the applied field, F is the electric force density, V is the crystal volume, and the angular brackets denote an ensemble average over crystal internal states.

Because both the force density F and the displacement u depend linearly upon the local polarization, one finds that the dissipation can be related directly to the spatial correlation function $\langle P(r_1)P(r_2)\rangle$. Our goal is to determine properties of this correlation function which will give rise to the observed microwave loss in the tungsten bronzes. If these prove consistent with experimental evidence from other sources, then a full dielectric theory, encompassing both the dispersion and loss along both crystal axes, will be attempted along these lines.

4.0 CONCLUSIONS AND RECOMMENDATIONS

The status of our investigations on the tungsten bronzes has now advanced to the point where various models for dn_i/dE_j can be tested. Preliminary results from free-space measurements on SBN:60 at room temperature and 77K suggest that the temperature dependence of dn_3/dE_3 (the polar axis sensitivity) at 90-100 GHz is much smaller than either the phonomenological model predictions based on low frequency behavior or the n^5 model of Boyd.

Our measurements of dn_1/dE_3 show the interesting feature that, even though the complex a-axis permittivity remains substantially constant over the temperature range, dn_1/dE_3 falls significantly at liquid nitrogen temperatures. This behavior is qualitatively consistent with predictions of the phenomenological model if ε_1 at the microwave frequency is constrained to be temperature insensitive.

These results are only a beginning, based on a limited exploration in temperature and frequency. We are now constructing a thermostatted enclosure for the ferroelectric samples; the enclosure will permit reliable measurements of dn/dE at any temperature between 77K and the Curie point for each sample.

The key factor which has led to these recent advances has been the availability of samples sufficiently large for free-space measurements. Over the last two years, we have discovered and verified that the small gaps necessary for dn/dE measurements in waveguides introduce substantial corrections to the transmitted power when the samples are lossy. One must circumvent the uncertainties connected with such corrections to obtain reliable values for dn/dE.

Our recommendations for the future direction of this program follow directly from this recent experience. Clearly, it will be advantageous to further develop crystals of a size suitable for unambiguous measurement of dn/dE over a range of frequency. The measurements should be carried out over a broad temperature range to obtain an accurate picture of the interrelationship of permittivity, polarization, and field sensitivity. These results, in

turn, will drive the development of new theories for the dielectric properties. Ultimately, the understanding provided by these investigations should lead to an evaluation of the potential of this whole class of materials for device applications based on electric-field induced changes in their properties.

5.0 FUTURE PLANNED RESEARCH WORK

We will continue to determine high frequency dielectric properties of various ferroelectric family crystals at room temperature as well as low temperature. The main objective is to identify the factors controlling the susceptibilities and especially the loss mechanisms in these ferroelectric materials. A brief outline of the future work is as follows:

1. Continue to establish growth techniques to develop existing and new ferroelectric materials.

2. Study low temperature and high frequency dielectric properties of selected materials.

3. Establish techniques to evaluate dn/dE and modulation behavior at low and high frequencies over a full range of temperature from T_c to 40K.

4. Continue to develop a suitable model to explain current high frequency dielectric properties in the tungsten bronzes and other crystals.

5. Develop device concepts utilizing the large values of dn/dE available in the tungsten bronzes.

5.1   Bulk Crystal Growth of Tungsten Bronze Crystals

In future work, we will continue to develop the current Czochralski technique equipped with the ADC system for KLN and some MPB compositions, e.g., BSNN, PBKNN. As discussed earlier, the growth of KLN crystals has been successful but needs further attention to improve crystal size and quality. The MPB systems selected in this work are also suitable for growth and will be studied.

5.2 Development of PBN by the Hot-Pressing Technique

Our initial work on tungsten bronze $Pb_{1-x}Ba_xNb_2O_6$ (PBN) has shown this material to be very promising for a number of applications, including piezoelectric, electro-optic, nonlinear optic and acousto-optic device applications. This solid solution possesses both orthorhombic and tetragonal forms, with a morphotropic phase boundary occurring at $x = 0.37$. The phase diagram for this system as a function of Ba^{2+} content has been established based on our previous work on ceramic and single crystal samples of this material, as shown in Fig. 9. Concurrent theoretical work has shown an enhancement of the ferroelectric properties of PBN near the morphotropic phase boundary between the ferroelectric orthorhombic (mm2) and ferroelectric tetragonal (4mm) structure near the composition $Pb_{0.6}Ba_{0.4}Nb_2O_6$. This has been experimentally verified using small single crystals grown by the Czochralski technique, as well as with ceramic samples.
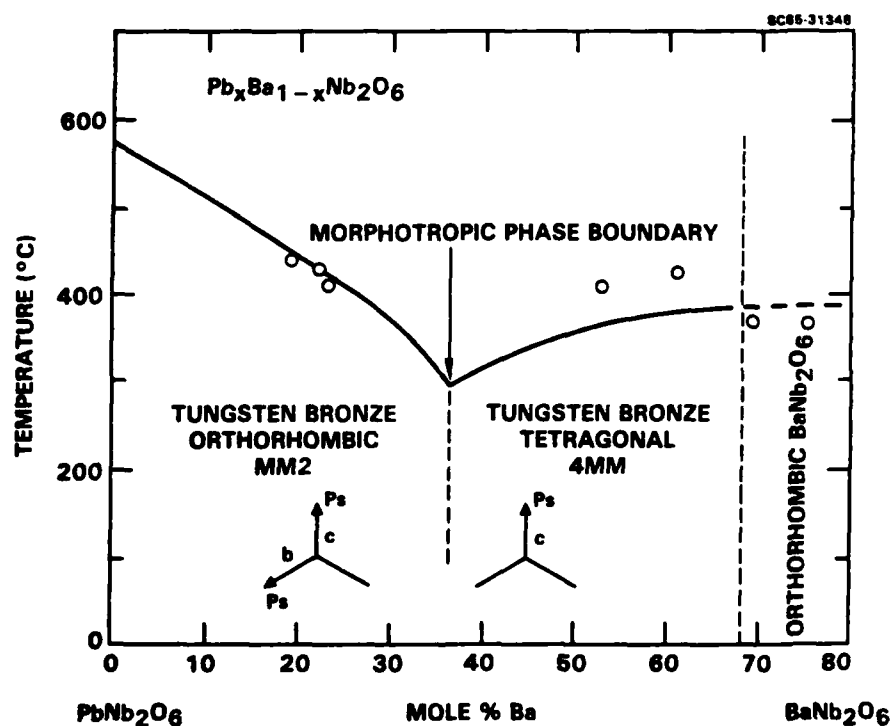

Fig. 9 Phase diagram for the solid solution $Pb_{1-x}Ba_xNb_2O_6$ as a function of x.

Although we have been able to grow small to medium sized single crystals of PBN (under DARPA contract at Penn State), growth is generally difficult for a number of reasons. These include loss of Pb^{2+} due to its high voltalization, compositional gradients in the grown crystals, and crystal cracking when cycling through the paraelectric/ferroelectric phase transition temperature. Figure 10 shows the ternary phase diagram established for this system. The alternative technique to this problem is the development of the ceramic hot-pressing technique which is now routinely used for perovskites and other compositions. Nagata and Okazaki[4] successfully demonstrated the growth of PBN compositions using the hot-pressing technique. This technique has been used in our own work for last several years; however, only recently has this growth been performed in an oxygen atmosphere. The results of this investigation indicate that the growth of transparent ceramic PBN is possible.
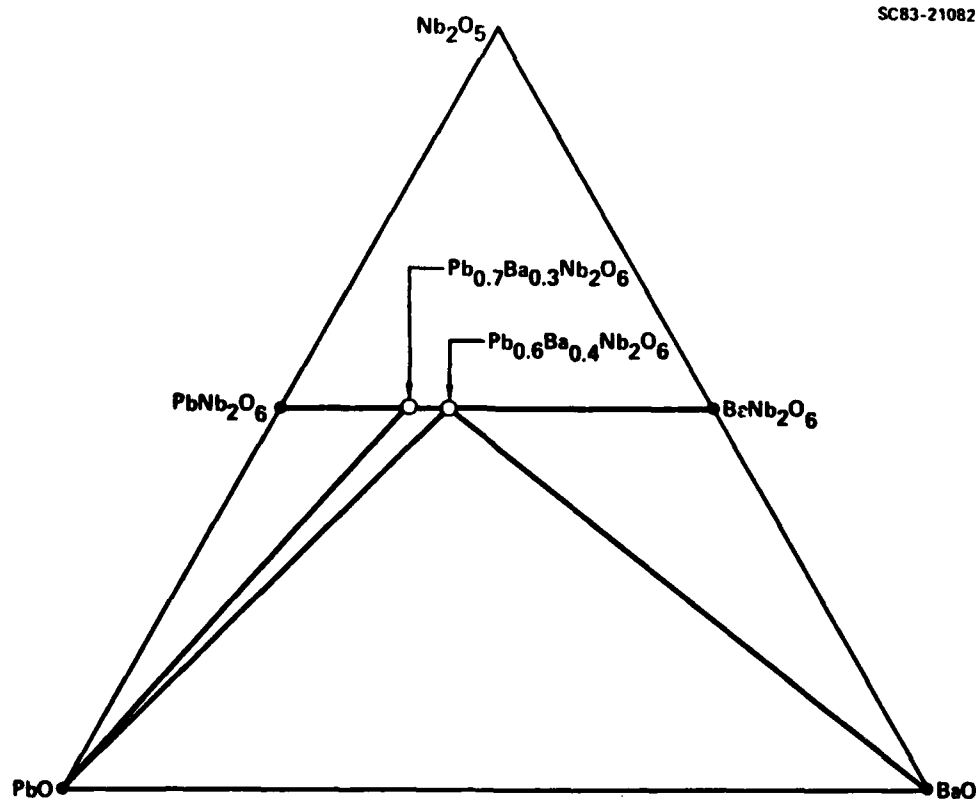
SC83-21082

Fig. 10 Ternary phase diagram for the system $PbO-BaO-Nb_2O_5$.

Figure 11 shows a transparent PBN dense ceramic grown under contract
IR&D and ONR sponsorship. Both the dielectric and electro-optic coefficients
for this composition are very high, and this composition is expected to be very
interesting for high frequency studies. During the next six months, the
following parameters will be studied in more detail:

1.   Establish conditions to develop completely transparent ceramics,
      approximately 1-2 in. in diameter.

2.   Study the role of dopants to enhance dielectric properties.

3.   Examine low and high temperature high frequency dielectric and
      conductivity properties.

4.   Extend the current technique to other important perovskite
      compositions, e.g., KTN, PZT, PLZT, etc.
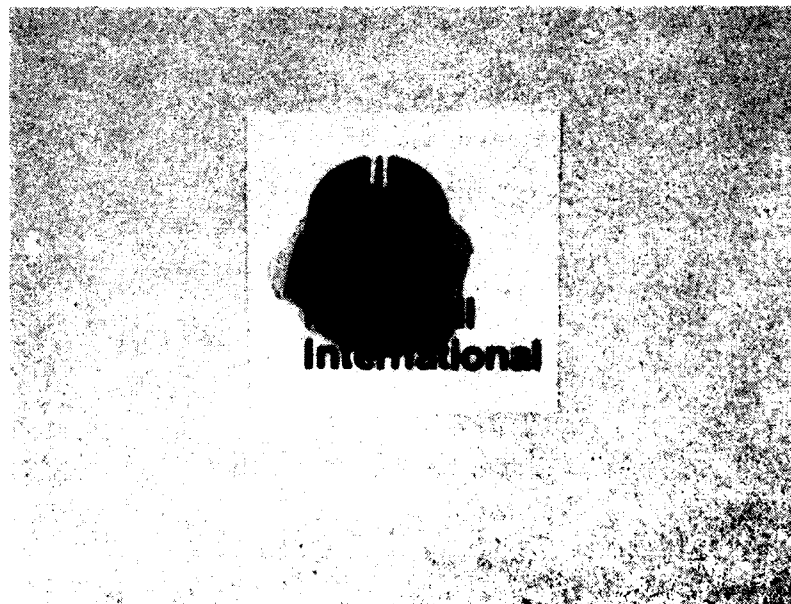
SC85-32903

Fig. 11 $Pb_{0.6}Ba_{0.4}Nb_2O_6$ dense ceramic formed by oxygen atmosphere
hot-pressing.

5.3   Measurements and Theoretical Modeling

Work will continue on the refinement of the measurement capabilities at both the Science Center and UCLA locations. At UCLA, plan to improve our apparatus for the determination of longitudinal and transverse electro-optic coefficients, and to extend these measurements to low temperatures. This will then be implemented in both planar and microstrip configurations in the more promising materials to explore practical device applications. At the Science Center, the apparatus will be modified to provide a more continuous temperature spectrum of the dielectric properties of these materials. Perhaps of primary importance at this point is the development of large sized BSKNN crystals for free-standing dielectric and dn/dE measurements, work which is on-going in the materials growth area of this program.

Much of the current theoretical work will be continued and modified as necessary based on experimental data. Parallel empirical modeling work is being done at the low frequency end of the spectrum (100 Hz-100 kHz), and it is hoped that some correlation between the two frequency extremes can be established to help unify the theoretical model and to solidify the mechanics involved in the dielectric properties of these materials.

6.0 PUBLICATIONS AND PRESENTATIONS

6.1 Publications

1. R.R. Neurgaonkar, J.R. Oliver and L.E. Cross, "Ferroelectric Properties of Tetragonal T.B. Crystals," Ferroelectrics, 56, 31-36 (1984).

2. R.R. Neurgaonkar, W.W. Ho, W.K. Cory, W.F. Hall and L.E. Cross, "Low and High Frequency Dielectric Properties of T.B. $Sr_2KNb_5O_{15}$ Crystals," accepted for publication in Ferroelectrics.

3. R.R. Neurgaonkar, W.K. Cory and J.R. Oliver, "Growth and Applications of Ferroelectric T.B. Family Crystals," Proceedings of the Southwest Conference on Optics, 1985.

4. W.W. Ho, W.F. Hall and R.R. Neurgaonkar, "Low Temperature High Frequency Dielectric Properties of T.B. Family Crystals," (in preparation).

6.2 Presentations

1. R.R. Neurgaonkar, "Tungsten Bronze Family Crystals for Optical Device Applications," presented at the SPIE-International Society for Optics Engineering Conference, Los Angeles, CA, Jan 26-27, 1984.

2. R.R. Neurgaonkar, "Epitaxial Growth of Ferroelectric Single Crystal Thin Films for Optical and Acoustical Applications," presented at the 3rd International Conference on Solid Films and Surfaces, Sydney, New South Wales, Australia, August 26-31, 1984.

3. R.R. Neurgaonkar, W.K. Cory and J.R. Oliver, "Growth and Applications of T.B. Family Crystals," presented at the SPIE Southwest Conference on Optics, Albuquerque, NM, March 4-8, 1985.

4. J.R. Oliver and R.R. Neurgaonkar, "Ferroelectric Solid Solutions Based on the T.B. Structure," presented at the 86th Annual Meeting of the American Ceramic Society, Pittsburgh, PA, April 1985.

7.0 REFERENCES

1. G.D. Boyd and M.A. Pollack, Phys. Rev. B $\underline{7}$, 5345 (1973).

2. L.E. Cross, private communication.

3. R.A. Toupin, Ph.D. Thesis, Syracuse University (1961).

4. K. Nagata and K. Okazaki, Japan-U.S. Study Seminar on Dielectric and Piezoelectric Ceramics, W-11 (1982).

APPENDIX 1

A PHENOMENOLOGICAL ANALYSIS OF TETRAGONAL TUNGSTEN BRONZE FERROELECTRICS

L.E. Cross and R.R. Neurgaonkar

A PHENOMENOLOGICAL ANALYSIS OF TETRAGONAL TUNGSTEN BRONZE FERROELECTRICS

L.E. Cross
Materials Research Laboratory
The Pennsylvania State University
University Park, PA 16802

R.R. Neurgaonkar
Rockwell Science Centre
Thousand Oaks, CA

ABSTRACT

A simple Devonshire form has been derived for the Phenomenological Elastic Gibbs Function to describe the elasto-dielectric parameters of simple proper ferroelectrics in the Tungsten Bronze Structure family which has 4/mmm prototypic point symmetry. For the assumption that all temperature dependence is carried by the Curie Weiss behaviour implicit in the quadratic term and that the expansion may be terminated at the first 6th order term reasonable agreement between calculated and derived P_s vs. T curves in the ferroelectric phase can be obtained for a wide range of bronze compositions.

From the fitting it is clear that second and sixth rank terms are remarkably constant over a very wide range of bronze compositions. Variation in the negative fourth rank term is larger, but this is to be expected since it contains large contributions from electrostrictive and elastic terms which will depend upon boundary conditions.

These initial studies suggest that the phenomenological method may be used to derive expectation values for tensor parameters across the whole family of ferroelectric bronzes. The study also points up the need for more careful detailed studied of lattice strain, birefringence and permittivity as a function of temperature in model bronze compounds to provide more detailed checks of the method.

1-2

1.0 INTRODUCTION

The Tungsten Bronze family of simple proper ferroelectrics incorporates now almost 100 different end member compositions, most of which are mutually compatible in solid solution, so that an immense range of possible ferroelectrics is available. In attempting to select compositions for device application in optics, nonlined optics, electrooptics, acoustooptics, SAW, etc., it is important for each device to maximize a different combination of the tensor properties of the crystal, so that some theoretical predictive capability would be of major help in making rational choices in this bewildering range of possible bronze compositions. For complex structures like the ferroelectric bronzes, however, where different cations can have different fractional occupancy on several sites in the structure, a rigorous atomistic theory is at present out of the question. It is the purpose of this paper to explore the extent to which thermodynamic phenomenological methods can be used to correlate the tensor properties to point up the inadequacies of present experimental data and to suggest a more systematic experimental approach.

A rather simple Landau:Ginsburgh:Devonshire function for the Elastic Gibbs Free Energy of simple proper ferroelectric bronzes which can be derived for the 4/mmm prototype symmetry has been discussed earlier (1), and the function was used with good results to fit the dielectric, electric and piezoelectric properties of the $Ba_{0.40}Sr_{0.60}Nb_2O_6$ (SBN) ferroelectric composition (2). A simple power series expansion up to the first 6th power terms in polarization but including only fourth rank terms in elastic and elasto-electric coupling terms proved adequate to explain dielectric, piezoelectric and spontaneous shape change data, however it was necessary to include sixth order electrostriction to model the elastic constant behaviour. The relaxor dielectric character of SBN was taken into account by using a

1-3

narrow distribution of Curie temperatures T_c, and did not obtrude in the fitting process except for properties very close to T_c where fluctuations in the polarization take P_3^2 far from zero (3).

2.0 THERMODYNAMIC PHENOMENOLOGY

Recapitulating our earlier studies, it has been the contention that an empirical thermodynamic elastic Gibbs function can be developed which will describe the polarization induced changes in the dielectric, elastic, thermal, piezoelectric and electro-optic properties in all possible simple proper ferroelectric phases of the tungsten bronze structure ferroelectrics.

Under the symmetry constraints of the 4/mmm point symmetry of the prototypic form of the bronzes, the permitted dielectric stiffnesses α_{ij}, fourth order stiffnesses α_{ijkl}, electrostriction constants Q_{ijkl} elastic compliances s_{ijkl} and sixth order dielectric stiffnesses α_{ijklmn} are listed in Tables I through IV.

Using the reduced notation 11 -> 1, 22 -> 2, 33 -> 3, 23 or 32 -> 4, 13 or 31 -> 5 and 12 or 21 -> 6 the elastic Gibbs function takes the form

$$\Delta G_1 = \alpha_1(P_1^2+P_2^2) + \alpha_3 P_3^2 + \alpha_{11}(P_1^4+P_2^4) + \alpha_{33}P_3^4$$

$$+ \alpha_{13}(P_1^2 P_3^2+P_2^2 P_3^2) + \alpha_{12}P_1^2 P_2^2 + \alpha_{333}P_3^6$$

$$+ \alpha_{111}(P_1^6+P_2^6) - \frac{1}{2} s_{11}(X_1^2+X_2^2) - s_{12}X_1 X_2$$

$$- s_{13}(X_1+X_2)X_3 - \frac{1}{2} s_{33}X_3^2 - \frac{1}{2} s_{44}(X_4^2+X_5^2)$$

$$- \frac{1}{2} s_{66}S_6^2 - Q_{11}(P_1^2 X_1+P_2^2 X_2) - Q_{12}(P_1^2 X_2+P_2^2 X_1)$$

$$- Q_{13}(P_1^2 X_3+P_2^2 X_3) - Q_{31}(P_3^2 X_1+P_3^2 X_2)$$

$$- Q_{33}P_3^2 X_3 - Q_{44}(P_2 P_3 X_4+P_1 P_3 X_5)$$

$$- Q_{66}P_1 P_2 X_6 \tag{1}$$

The first partial derivatives with respect to the polarization give the field components

$$\frac{\partial \Delta G}{\partial P_1} = E_1 \; 2a_1 P_1 + 4a_{11} P_1^3 + 2a_{13} P_1 P_3^2$$

$$+ 2a_{12} P_1 P_2^2 + 6a_{111} P_1^5$$

$$+ Q_{13} P_1 X_3 + Q_{44} P_3 X_5 + Q_{66} P_1 X_6 \tag{2}$$

$$\frac{\partial \Delta G}{\partial P_2} = E_2 = 2a_1 P_2 + 4a_{11} P_2^3 + 2a_{13} P_2 P_3^2$$

$$+ 2a_{12} P_2 P_1^2 + 6a_{111} P_2^5$$

$$+ 2Q_{13} P_2 X_3 + Q_{44} P_3 X_4 + Q_{66} P_1 X_6 \tag{3}$$

$$\frac{\partial \Delta G}{\partial P_3} = E_3 = 2a_3 P_3 + 4a_{33} P_3^3 + 2a_{13}(P_1^2 + P_2^2) P_3$$

$$+ 6a_{33} P_3^5 + 2Q_{31} P_3 (X_1 + X_2)$$

$$+ 2Q_{33} P_3 X_3 + Q_{44}(P_2 X_4 + P_1 X_5) \tag{4}$$

It is the solutions of these equations with $E_i = 0$ which determine the ferroelectric states for a free crystal ($X = 0$). In general, there are seven possible ferroelectric species which can occur from the prototypic 4/mmm symmetry of the paraelectric phase of the tungsten bronze, each of which corresponds to a different combination of non-zero (spontaneous) values of the P_i components. All possible solutions for the three equations (2-4) were derived and reported by Cross and Pohanka (1968). Practically, however, just two of these solutions encompass all presently known simple ferroelectric bronzes. These are

(a) $P_3^2 \neq 0$ $\qquad$ $P_1 = P_2 = 0$

(b) $P_1^2 = P_2^2 \neq 0$ $\qquad$ $P_3 = 0$.

The species (a) corresponds to the Shuvalov (1970) species 4/mmm (1) D4 F4mm where 4/mmm is the high temperature prototype point group and F4mm means that the crystal is ferroelectric of point group 4mm below the transition temperature. D(4) indicates that the spontaneous polarization P_s has definite orientation along the four-fold symmetry axes, and (1) denotes number of equivalent four-fold axis which is one. In other words, there are two domains of opposite orientation of P_s (i.e., $180°$ domains) along the four-fold prototypic axis. The second species (b) is one of the subtypes of 4/mmm (2)D2 Fmm2 with P_s along the two-fold axis which make angles of $45°$ with 1 and 2 prototype axis ($P_1^2 = P_2^2$) and has four equivalent ferroelectric domain states.

Substituting the conditions (a) into the general equations (2-4) gives the following conditions for stability:

$$P_1 = P_2 = 0 \qquad 0 = 2a_3 + 4a_{33}P_3^2 + 6a_{333}P_3^4 \qquad (5)$$

The isothermal dielectric stiffness χ_{ij} are

$$\chi_{11}^T = 2a_1 + 2a_{13}P_3^2$$
$$\chi_{22}^T = 2a_1 + 2a_{13}P_3^2$$
$$\chi_{33}^T = 2a_3 + 12a_{33}P_3^2 + 30a_{333}P_3^4$$
$$\chi_{12}^T = \chi_{13}^T = \chi_{23}^T = 0 \qquad (6)$$

The tetragonal spontaneous strains are given by

$$x_1 = Q_{31}P_3^2 \qquad x_4 = x_5 + x_6 = 0$$
$$x_2 = Q_{31}P_3^2$$
$$x_3 = Q_{33}P_3^2 \qquad (7)$$

and the piezoelectric b coefficients by

$$b_{11} = 0 \qquad b_{21} = 0 \qquad b_{31} = 2Q_{31}P_3$$

$$b_{12} = 0 \qquad b_{22} = 0 \qquad b_{32} = 2Q_{31}P_3$$

$$b_{13} = 0 \qquad b_{23} = 0 \qquad b_{33} = 2Q_{33}P_3$$

$$b_{14} = 0 \qquad b_{24} = Q_{44}P_3 \qquad b_{44} = 0$$

$$b_{15} = Q_{44}P_3 \qquad b_{25} = 0 \qquad b_{35} = 0$$

$$b_{16} = 0 \qquad b_{26} = 0 \qquad b_{36} = 0 \qquad\qquad (8)$$

For the case (b) the corresponding equations take the form, for the stability conditions,

$$P_1^2 = P_2^2 \qquad 0 = 2a_1 + (4a_{11}+2a_{12})P_1^2 + 6a_{111}P_1^4$$

$$P_3 = 0 \qquad\qquad (9)$$

Isothermal stiffnesses are

$$\chi_{11}^T = 2a_1 + 12a_{11}P_1^2 + 2a_{12}P_1^2 + 30a_{111}P_1^4$$

$$\chi_{22}^T = 2a_1 + 12a_{11}P_1^2 + 2a_{12}P_1^2 + 30a_{111}P_1^4$$

$$\chi_{33}^T = 2a_3 + 4a_{13}P_1^2$$

$$\chi_{34}^T = 4a_{12}P_1^2 \qquad \chi_{13} = \chi_{23} = 0 \qquad\qquad (10)$$

It may be noted that the coefficients here are expressed with respect to the original prototypic axes and thus satisfy pseudomonoclinic symmetry. However, a simple rotation of the matrix by 45° in the 1,2 plane would reveal the true orthorhombic symmetry.

Spontaneous elastic strains take the form

$$x_1 = (Q_{11}+Q_{12})P_1^2$$

$$x_2 = (Q_{11}+Q_{12})P_1^2$$

$$x_3 = 2Q_{13}P_1^2$$

$$x_6 = Q_{66}P_1^2 \qquad x_4 = x_5 = 0 \qquad\qquad (11)$$

and the piezoelectric coefficients are

$$b_{11} = 2Q_{11}P_1 \qquad b_{21} = 2Q_{12}P_1 \qquad b_{31} = 0$$

$$b_{12} = 2Q_{12}P_1 \qquad b_{22} = 2Q_{11}P_1 \qquad b_{32} = 0$$

$$b_{13} = 2Q_{13}P_1 \qquad b_{23} = 2Q_{13}P_1 \qquad b_{33} = 0$$

$$b_{14} = 0 \qquad b_{24} = 0 \qquad b_{34} = Q_{44}P_1$$

$$b_{15} = 0 \qquad b_{25} = 0 \qquad b_{35} = Q_{44}P_1$$

$$b_{16} = Q_{66}P_1 \qquad b_{26} = Q_{66}P_1 \qquad b_{36} = 0 \tag{12}$$

Table I

Equivalent Second and Fourth Rank Dielectric Terms for 4/mmm Symmetry

Nye's Matrix Notation		Full Tensor Notation		Number of Equivalent Terms
Term	Symmetry Equivalent Terms	Term	Symmetry Equivalent Terms	
α_1	α_2	α_{11}	α_{22}	2
α_3		α_{33}		1
α_{11}	α_{22}	α_{1111}	α_{2222}	2
α_{12}	α_{21}, α_{66}	α_{1122}	$\alpha_{1212}, \alpha_{1221}, \alpha_{2112},$ $\alpha_{2121}, \alpha_{2211}$	
α_{13}	$\alpha_{31}, \alpha_{23}, \alpha_{32}, \alpha_{44}, \alpha_{55}$ ($\alpha_{44} = 4\alpha_{2323}$)	α_{1133}	$\alpha_{3311}, \alpha_{2233}, \alpha_{1313},$ $\alpha_{1313}, \alpha_{1331}, \alpha_{3113},$ $\alpha_{3131}, \alpha_{2323}, \alpha_{2332},$ $\alpha_{3223}, \alpha_{3232}$	12
α_{33}		α_{3333}		1

Table II

Equivalent Electrostriction Terms for 4/mmm Symmetry

| Nye's Matrix Notation | | Full Tensor Notation | | Number of |
Term	Symmetry Equivalent Terms	Term	Symmetry Equivalent Terms	Equivalent Terms
Q_{11}	Q_{22}	Q_{1111}	Q_{2222}	2
Q_{12}	Q_{21}	Q_{1122}	Q_{2211}	2
Q_{13}	Q_{23}	Q_{1133}	Q_{2233}	2
Q_{31}	Q_{32}	Q_{3311}	Q_{3322}	2
Q_{33}		Q_{3333}		1
Q_{44}	Q_{45}	Q_{2323}	Q_{2332}, Q_{3223}, Q_{3232}, Q_{1313}, Q_{1331}, Q_{8113}, Q_{3151}	8
Q_{66}		Q_{1212}	Q_{1221}, Q_{2112}, Q_{2121}	4

Table III

Equivalent Elastic Compliance Terms for 4/mmm Symmetry

	Nye's Matrix Notation	Full Tensor Notation		Number of
Term	Symmetry Equivalent Terms	Term	Symmetry Equivalent Terms	Equivalent Terms
s_{11}	s_{22}	s_{1111}	s_{2222}	2
s_{12}	s_{21}	s_{1122}	s_{2211}	2
s_{13}	s , s_{23}, s_{32}	s_{1133}	s_{3311}, s_{2233}, s_{3322}	4
s_{33}		s_{3333}		1
s_{44}	s_{55}	s_{2323}	s_{2332}, s_{3223}, s_{3232}, s_{1313}, s_{1331}, s_{3113}, s_{3131}	8
s_{66}		s_{1212}	s_{1221}, s_{2112}, s_{2121}	4

Table IV

Equivalent Sixth Rank Tensor Terms of the Form $\alpha(P^6)$
for 4/mmm Symmetry

	Term	Symmetry Related Terms	Number of Equivalent Terms
1.	α_{111}	222	2
2.	α_{112}	166, 121, 616, 661, 211, 221, 266, 212, 626, 662, 122	30
3.	α_{113}	155, 131, 515, 551, 331, 223, 244, 232, 424, 442, 322	30
4.	α_{123}	144, 132, 525, 645, 546, 636, 663, 564, 654, 552, 321, 441, 231, 465, 366, 255, 456, 213, 414, 312	90
5.	α_{133}	535, 553, 331, 355, 313, 233, 434, 443, 332, 344, 323	30
6.	α_{333}		1

3.0 POTENTIAL UTILITY OF THE PHENOMENOLOGICAL THEORY

3.1 Introduction

It is evident from Tables I through IV that a substantial number of constants are required to characterize the bronzes in this phenomenological manner. The only formal benefit is that all the elasto-dielectric parameters of the lower symmetry ferroelectric forms can be characterized in terms of the nonlinear parameters of the higher symmetry prototype form.

In principle, it is possible that all the parameters can be functions of both temperature and composition, however, several pieces of evidence, both direct and indirect suggest that:

(a) The dominant temperature dependence is carried in the terms α_1 and α_3 which have a Curie Weiss form

$$\alpha_1 = \alpha_{10} \ (T-\theta_1)$$
$$\alpha_3 = \alpha_{30} \ (T-\theta_3).$$

(13)

(b) The higher order constants do not change markedly with either temperature or composition across a wide field of compounds and solid solutions with bronze structure.

In earlier studies we have demonstrated

(i) That in all known ferroelectric bronzes, only two of the seven possible ferroelectric species which are available from the 4/mmm prototype occur in nature.

(ii) In the tetragonal ferroelectric form in $(Sr_{0.61}Ba_{0.39})Nb_2O_6$ which is the congruently melting SBN composition, the data followed very closely to the phenomenology except for temperature close to the Curie point T_c and all parameters have been evaluated.

(iii) For the $(Pb_{1-x}Ba_x)Nb_2O_6$ compositions in the tetragonal phase field but close to the morphotropic phase boundary at the $(Pb_{0.6}Ba_{0.4})Nb_2O_6$ composition, the dielectric, piezoelectric and electro-optic behavior can be

1-13

quite accurately modeled using the phenomenological constants for SBN and just adjusting θ_1 and Q_3 to conform to the observed Curie Weiss behavior in these compositions (4).

The success to date with the modeling suggest that we attempt a more ambitious assessment of the range of validity of our simple hypotheses (a) and (b) above using a much wider range of bronze compounds and making use of literature values to evaluate directly, wherever possible, the stiffness parameters. The results of this effort will form the bulk of this paper.

A second feature which has become evident from our modeling of the tungsten bronze ferroelectrics is that particularly in the elastic response, the relaxor character of the bronzes is reflected in a breakdown of the static phenomenological model at temperatures close to T_c due to the onset of fluctuations in P. Thus for a range of temperatures above T_c it is evident that though $\bar{P} = 0$, is rigorously true $\bar{P^2} \neq 0$. The onset of a substantial fluctuating component in P will clearly affect all parameters which depend on even powers of P such as the linear dimensions, since

$$x_{ij} = Q_{ij33}P_3^2 \tag{14}$$

the optical refractive index as

$$\Delta B_{ij} = g_{ij33}P_3^2 \tag{15}$$

and the elastic compliance

$$s_{ijkl} = \phi_{ijkl33}P_3^2 \tag{16}$$

Perhaps the easiest to analyze is the strain response, and this will be the subject of a subsequent paper.

3.2 Evaluation of the Thermodynamic Parameters

In spite of the fact that more than 100 different ferroelectric compounds with the tungsten bronze structure have been synthesized, and innumerable solid solutions can be made between these end member compositions, there is a genuine paucity of reliable experimental data from which to evaluate the thermodynamic constants. For many materials, only ceramic samples have been made and in these, it is impossible to separate the individual tensor components. Even in many systems where good single crystals have been grown, the headlong rush to print has left many of the important parameters unmeasured.

For this study we have been able to find adequate but incomplete data for several $Ba_xSr_{1-x}Nb_2O_6$ solid solutions. In several $La_2O_3:KSr_2Nb_5O_{15}$ compounds and solid solutions and for pure $KSr_2Nb_5O_{15}$ there is also adequate though incomplete data. $NaBa_2Nb_5O_{15}$ may be analysed on this model if the weak ferroelastic phase change near 370°C is neglected, and there is some data for a titanium modified $NaBa_2Nb_5O_{15}$. Similarly in $K_3Li_2Nb_5O_{15}$ there is adequate data for some of the constants though the transverse dielectric response has apparently not been measured.

In the orthorhombic ferroelectric form, we have only been able to find data for $PbNb_2O_6$ and for $Pb_2KNb_5O_{15}$. The fitting to obtain the thermodynamic parameters is, however, more difficult in these compositions and will be covered in a subsequent paper.

For the tetragonal ferroelectric form, the evaluation is relatively straight-forward. The constant a_3 has the form $a_3 = a_{30}(T-\theta_3)$ which leads to an equation for the stiffness χ_{33} above T_c of the form

$$\chi_{33} = 2a_{30}(T-\theta_3) \tag{17}$$

Thus the extrapolation of the Curie Weiss plot of stiffness above T_c gives the temperature θ and the slope in the constant $2a_{30}$.

By equating the ΔG values in ferroelectric and paraelectric states at T_c, the equation for P_s (5) can be put into the Devonshire form

$$\frac{T-\theta}{T_c-\theta} - 4(\frac{P_3}{P_{30}})^2 + 3(\frac{P_3}{P_{30}})^4 = 0 \tag{18}$$

in which $T_c-\theta$ and P_{30} are the only fitting parameters.

Often, unfortunately, the published P_s vs T data for ferroelectric crystals is unreliable particularly at temperatures remote from T_c where it is often difficult to pole to a single domain state. Thus it is wise to check the shape of the polarization function by using a less direct method, e.g. the spontaneous strains $\Delta c/c$, $\Delta a/a$ induced in the ferroelectric form are electrostrictive in nature and thus scale with P_s^2. Similarly the optical impermeability changes below T_c (ΔB_{11} and ΔB_{33}) are again quadratic and scale with P_s^2. Piezoelectric b_{ij} constants on the other hand, being morphic, scale directly with P_s, as does the linear electro-optic effect and the nonlinear Miller δ coefficients.

A typical fitting of the different P_s data for $Ba_2NaNb_2O_6$ is shown in Figure 1. Clearly the Devonshire form is in excellent agreement with the 'birefringence' data which are probably most reliable in this crystal. From the values of T_c, θ, P_{so} and χ_{30} the α constants are given by

$$a_3 = 1/2 \ a_{30}(T_c-\theta_3) \tag{19}$$

$$a_{33} = - \frac{a_{30}(T_c-\theta_3)}{P_{so}} \tag{20}$$

$$a_{333} = \frac{a_{30}(T_c-\theta_3)}{2(P_{so})^4} \tag{21}$$

1-16

For the constant α_1 and α_{13} dielectric data for a section parallel to the c axis (ε_a) is required. Above T_c

$$\chi_1 = 2\alpha_{10}(T-\theta_1) \tag{22}$$

so that $2\alpha_{10}$ is the Curie Weiss slope and θ_1 the extrapolated Curie temperature.

To derive α_{13} it is then a simple matter to make use of equation (10) to obtain by least squares method a best fit to the experimental data below T_c, taking now calculated values for P_3 vs T.

A typical plot comparing measured and calculated values for $NaBa_2Nb_5O_{15}$ is given in Figure 2.

Using these methods constants for the bronze compositions derived are listed in Table V.

3.3 Discussion

It may be noted at once that for α_{30} and α_{333} there is excellent agreement over a very wide range of bronze compositions. The constant α_{10} is also within a narrow range, though here the stiffness is much larger and the Curie Weiss slope more difficult to read precisely. The α_{33} values cover a wider range and this also is perhaps not surprising. In the elastic Gibbs function, the negative value of α_{33} comes about because of a strong contribution from elastic and electrostrictive constants in the free crystal. Thus the magnitude of α_{33} is markedly dependent on the elastic boundary conditions and probably therefore on the crystal perfection. The α_{13} values also cover a rather wider range, but here the error is probably in the evaluation.

In summary, it does appear from these preliminary data that the original hypothesis of a constancy of the higher order stiffnesses is a good approximation for the tetragonal bronze ferroelectrics, and thus can form a
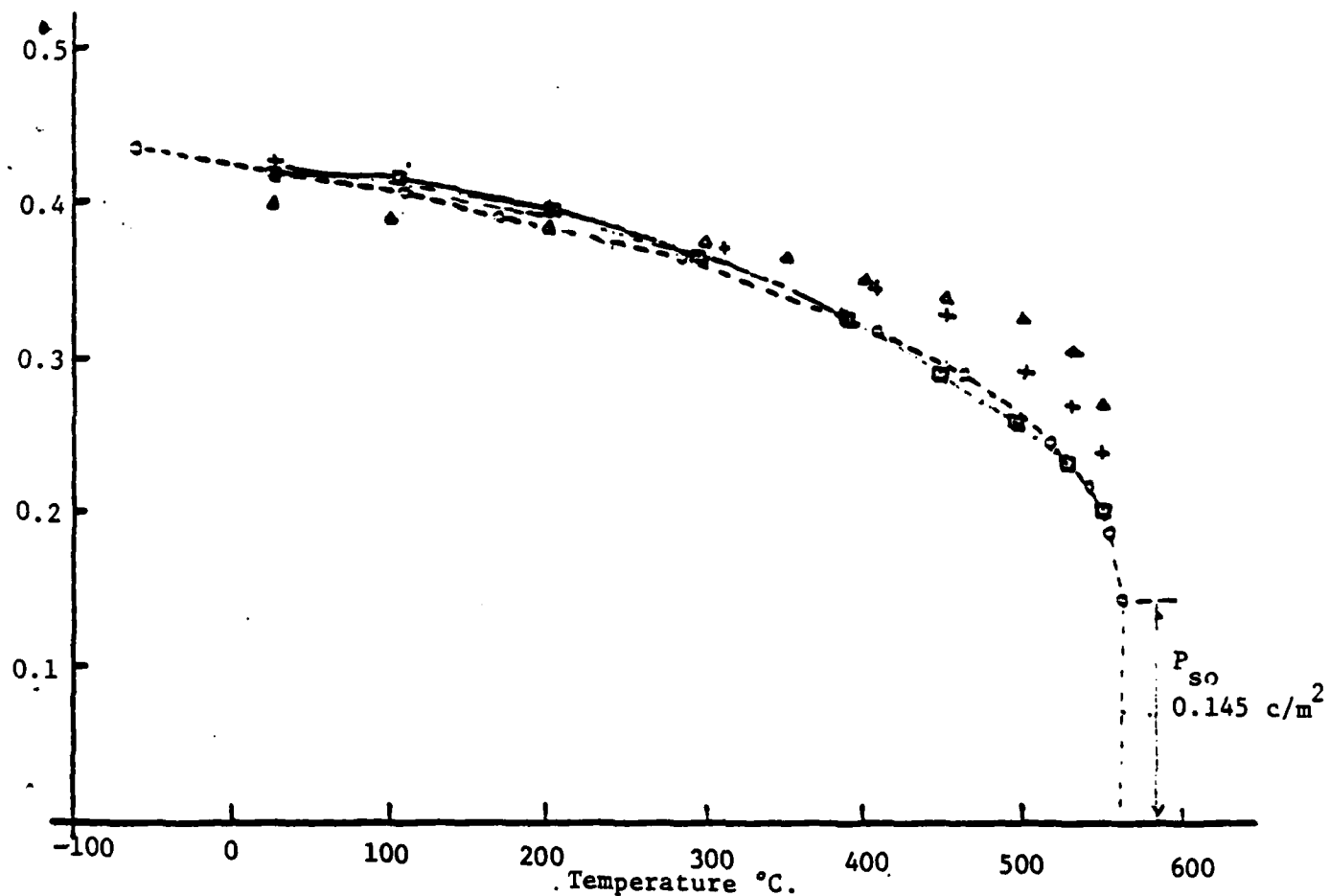
1-17

Figure 1. Phenomenological fitting of P_s vs T in $NaBa_2Nb_5O_{15}$.

o   o   o   Phenomenology
Δ   Δ   Δ   Nonlinear Optical Results
+   +   +   Pyroelectric Measurement
                   Optical Impermeability
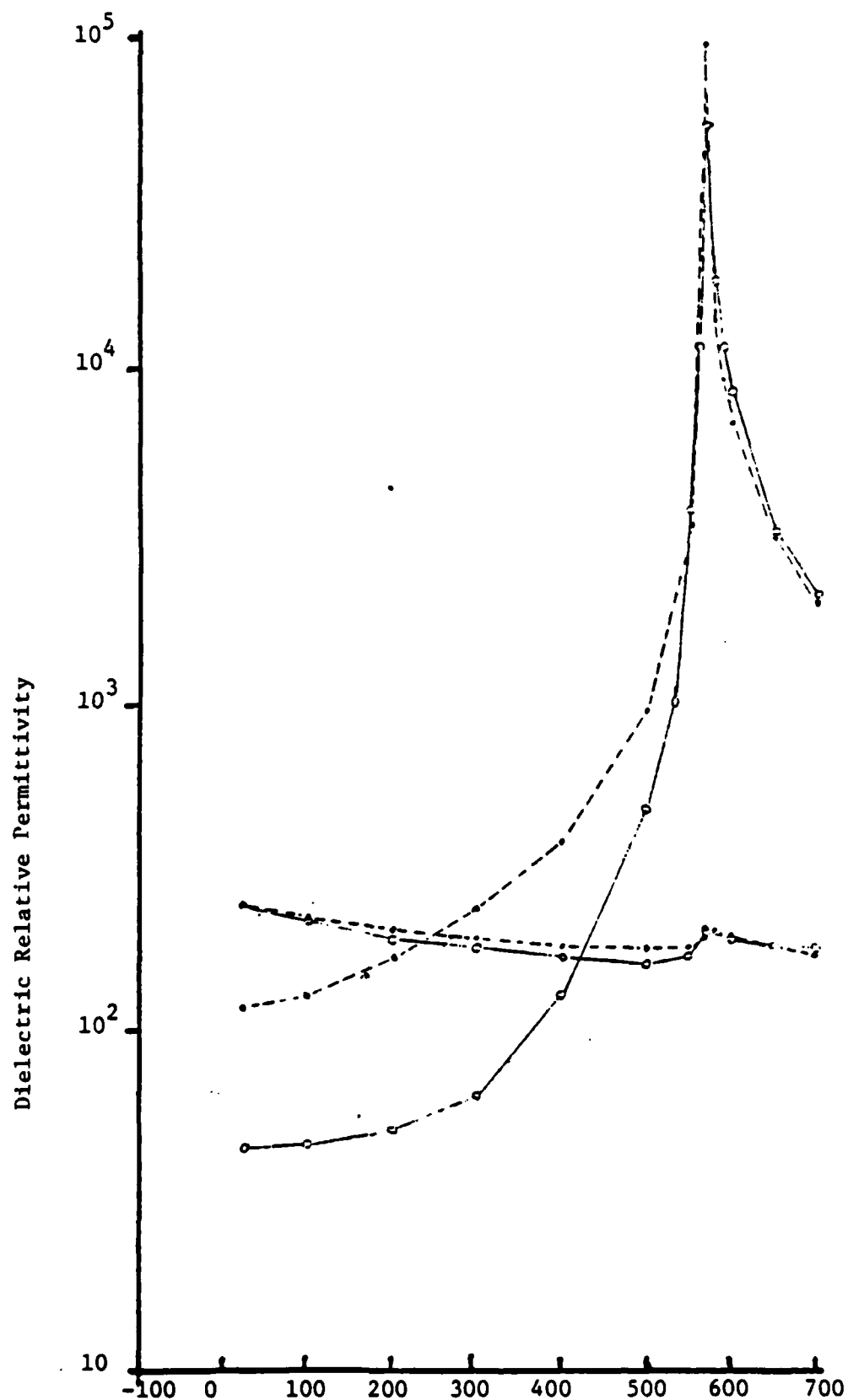
T_c = 563°C.
θ_3 = 560°C.
P_{so} = 0.145 c/m².

1-18

Figure 2. Phenomenological fitting to the dielectric permittivity in single crystal $Ba_2NaNb_5O_{15}$.

. . . Theory.
o o o Experiment.

Table V. Thermodynamic Constants for Tetragonal Tungsten Bronze Ferroelectric Crystals.

Compound	$1/2\ \alpha_{30}$	$12\ \alpha_{33}$	$30\ \alpha_{333}$	$1/2\ \alpha_{10}$	α_{13}
$Ba_{0.75}Sr_{0.25}Nb_2O_6$	$2.4\ 10^{-6}$	$-2.3\ 10^{-3}$	$3.6\ 1^{-1}$		
$Ba_{0.5}Sr_{0.5}Nb_2O_6$	$2.4\ 10^{-6}$	$-6.2\ 10^{-3}$	$3.2\ 10^{-1}$		
$Ba_{0.4}Sr_{0.6}Nb_2O_6$	$1.6\ 10^{-6}$	$-11.0\ 10^{-3}$	$3.6\ 10^{-1}$		
$Ba_{0.33}Sr_{0.67}Nb_2O_6$	$2.7\ 10^{-6}$	$-1.6\ 10^{-3}$	$3.1\ 10^{-1}$		
$Ba_{0.39}Sr_{0.61}Nb_2O_6$	$2.52\ 10^{-6}$	$-8.4\ 10^{-3}$	$3.6\ 10^{-1}$	$3.73\ 10^{-6}$	$2.1\ 10^{-3}$
$KSr_2Nb_5O_{15}$	$3.45\ 10^{-6}$	$-9.7\ 10^{-3}$	$3.4\ 10^{-1}$	$2.4\ 10^{-6}$	$11.3\ 10^{-3}$
3% (La) $KSr_2Nb_5O_{15}$	$2.2\ 10^{-6}$	$-9.6\ 10^{-3}$	$2.85\ 10^{-1}$		
6% (La) $KSr_2Nb_5O_{15}$	$2.0\ 10^{-6}$	$-10.5\ 10^{-3}$	$3.8\ 10^{-1}$		
9% (La) $KSr_2Nb_5O_{15}$	$3.14\ 10^{-6}$	$-12.2\ 10^{-3}$	$3.58\ 10^{-1}$		
$NaB_2Nb_5O_{15}$	$3.44\ 10^{-6}$	$-11.46\ 10^{-3}$	$2.5\ 10^{-1}$	$5.15\ 10^{-6}$	$13.3\ 10^{-3}$
$Na_{1.65}Ba_{4.35}Nb_{9.65}Ti_{0.35}O_{30}$	$3.56\ 10^{-6}$	$-5.34\ 10^{-3}$	$1.63\ 10^{-1}$		
$K_3Li_2Nb_5O_{15}$	$2.87\ 10^{-6}$	$-14.16\ 10^{-3}$	$1.13\ 10^{-1}$	$2.82\ 10^{-6}$	

basis for the analysis of the properties of a very wide range of bronze compositions.

REFERENCES

(1) L. E. Cross, R. Betsch, H. McKinstry, T. Shrout, R. R. Neurgaonkar. Proc. 34th Frequency Control Symp., May 1980.

(2) T. R. Shrout, L. E. Cross, P. Moses, H. A. McKinstry, R. R. Neurgaonkar. Proc. 1980 Ultrasonics Symp. 414, 1980.

(3) T. R. Shrout, "A Phenomenological Theory for Predicting the Temperature Dependence of Elastic Compliance in Simple Proper Ferroelectric Tungsten Bronzes," Ph.D. Thesis in Ceramic Science, The Pennsylvania State University, May 1981.

(4) T. R. Shrout, D. A. Hukin, L. E. Cross. Ferroelectric Letters 44, 325 (1983).

APPENDIX 2

ELECTRO-OPTIC DEVICES FOR MILLIMETER WAVE USING COOLED FERROELECTRICS

B. Bobbs, M. Matloubian, H. Fetterman, R.R. Neurgaonkar and W.K. Cory

Electrooptic devices for millimeter waves using cooled ferroelectrics

Bradley Bobbs, Mehran Matloubian & Harold R. Fetterman

Department of Electrical Engineering, University of California
Los Angeles, California 90024

Ratnakar R. Neurgaonkar & Warren K. Cory

Rockwell International Science Center
1049 Camino dos Rios, Thousand Oaks, California 91360

Abstract

The complex dielectric constants of two ferroelectric crystals SBN and BSKNN have been determined for millimeter waves betweeen 55 and 110 GHz as a function of temperature. These measurements used Fabry-Perot fringes produced by crystal surface reflections. Absorption was found to decrease markedly upon cooling for incident waves polarized along the crystal polar axis. Since exploitation of the large millimeter wave electooptic coefficients in these crystals is limited at room temperature by absorption losses, these reaults indicate that cooled crystals can be used for efficient low-loss electrooptic devices.

Introduction

Ferroelectric materials have shown great promise for use in devices in which an electrical signal controls millimeter waves by means of the linear electrooptic (Pockels) effect.[1-3] Amplitude or phase modulators, beam steerers, tunable bandpass filters and tunable antennas are examples of such devices. The materials with the largest electrooptic coefficients, $BaTiO_3$[4] and $Sr_{.61}Ba_{.39}Nb_2O_6$ (SBN)[5], however, have large absorption losses which limit their usefulness in practical devices. $BaTiO_3$ has the additional disadvantage that high quality single domain crystals are difficult to obtain, and are readily damaged or depoled; whereas SBN and other ferroelectrics in the tungsten bronze family, such as $Ba_{2-x}Sr_x K_{1-y}Na_yNb_5O_{15}$ (BSKNN), have been produced in consistently high quality, stable single domain crystals.[6-7] The present paper reports that a substantial decrease in absorption of millimeter waves by SBN and BSKNN may be achieved by cooling to cryogenic temperatures. Under these low-loss conditions, more efficient electrooptic devices can be developed.

Experimental method

Transmittance spectra over a full millimeter wave band may be measured at room temperature for small samples with high dielectric constant by means of an apparatus shown schematically in Figure 1.[8] The frequency of the narrowband output of a backward wave oscillator is stepped across the full band by a computer which also records the transmitted power measured by a thermistor-type detector. Normalization of the transmitted power spectrum by the power spectrum taken when the sample is removed cancels the effects of spectral variations in all components other than the sample. Parallel sample surfaces contact two waveguide flanges, with pressure maintained by small springs. The use of single mode hollow metal rectangular waveguide throughout maintains the linearly polarized TE_{10} mode,
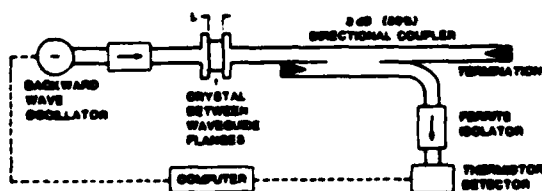

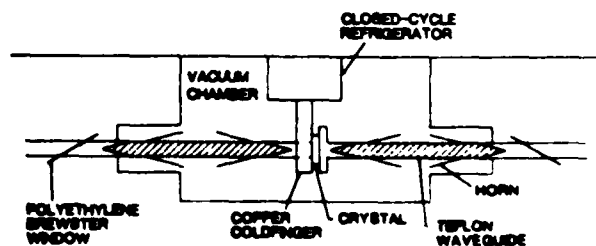Figure 1. Room temperature millimeter wave transmittance spectrum apparatus.

Figure 2. Sample mounting for low temperature measurements.

everywhere except possibly inside the sample and the isolators and directional coupler serve to eliminate extraneous standing waves.

The apparatus is extended to low temperature measurement by means of the sample mounting arrangement shown schematically in Figure 2. One of the waveguide flanges contacting the sample is soldered to a copper block attached to a closed cycle helium refrigerator unit. The unit is inside a mechanically pumped vacuum chamber to prevent vapor condensation and heat convection. Thin polyethylene vacuum windows are placed between metal waveguide sections cut approximately at the Brewster angle for the linearly polarized radiation, to minimize reflections which cause extraneous standing waves. A barrier to heat conduction along the waveguides is provided by sections of solid teflon rectangular waveguide which slide inside the metal waveguide. A two-step transition from hollow metal to teflon-filled metal to teflon alone is made by a pyramidal teflon taper and a metal horn, with low reflection and absorption losses. In this configuration the lowest sample temperature achievable is around 40K, and a heater and diode temperature sensor mounted on the copper block and connected to a computer-interfaced controller allows stabilization at any temperature up to 270K.

A sample with large millimeter wave dielectric constant will have large reflections off its entrance and exit faces which form Fabry-Perot interference fringes in the spectrum. The "optical" constants n and k (real and negative imaginary parts respectively of the complex refractive index) of the sample may then be determined by comparison of the experimental spectrum with theoretical Fabry-Perot spectra. The theory uses Fresnel reflection coefficients for the air-dielectric interfaces, modified by the change in phase velocity produced by the presence of the metal waveguide walls.[10] An example of a theoretical fit is shown as the solid line in Figure 3. The dotted line shows combined data over two millimeter wave bands for BSKNN at 40K with the crystal polar ("c") axis parallel to the radiation electric field. The rapid oscillations seen are not noise, but are reproducible, and are apparently caused by spectral variations in the coupling into and out of higher order transverse modes inside the sample. These oscillations are ignored in determining the theoretical fit.
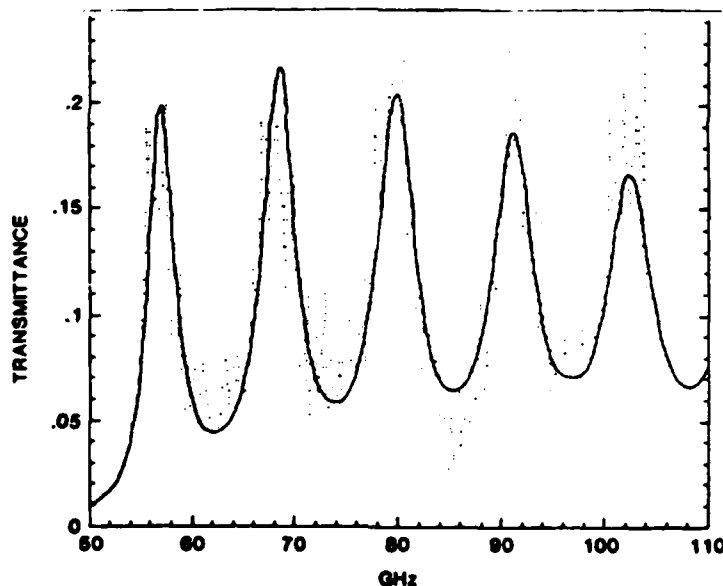

Figure 3. Experimental spectrum (dotted line) and theoretical
fit (solid line) for BSKNN axis at 40K.

The complex dielectric constant may be obtained from the optical constants simply by squaring the complex refractive index. The tangent of the phase δ of this quantity expressed in polar form is the loss tangent and the absorption coefficient is $4\pi k$ divided by the vacuum wavelength.

Results

Spectra were taken over the 55 to 85 GHz range for both SBN and BSKNN, and additionally over the 75 to 110 GHz range for BSKNN. Good fits were obtained by assuming constant values of n and k over the spectrum, although somewhat better fits could be obtained by allowing k to have a small spectral dependence, increasing linearly with frequency. The uncertainties

in n ranged from around ±1% for low absorption cases to 5% for high absorption.
Uncertainties for k were around twice that for n.

In SBN, for the a-axis (millimeter wave electric field perpendicular to crystal polar
axis), the complex refractive index n-ik was found to change from 18-1.3i at 290K to
16.5-0.63i at 40K, showing a significant decrease in absorption upon cooling. For the
c-axis (field parallel to polar axis), however, the change from n-3i (n could not be deter-
mined due to the lack of fringes) at 290K to 6.5-0.19i at 40K shows a decrease in absorption
which is quite dramatic.

Similar results were obtained for BSKNN. For the a-axis, the complex index of
17.3-0.72i at 290K showed no measurable change upon cooling. Spectra were taken at several
temperatures for the c-axis, with the n and k results shown in Figures 4 and 5. Over-
all it is seen that the absorption is significantly less than for SBN.
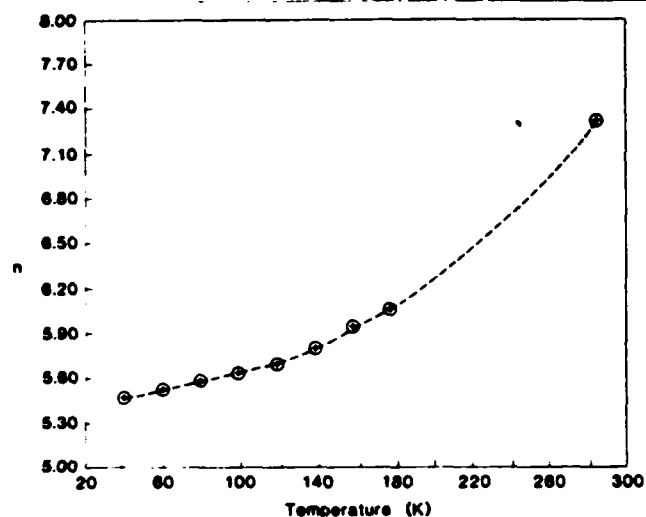

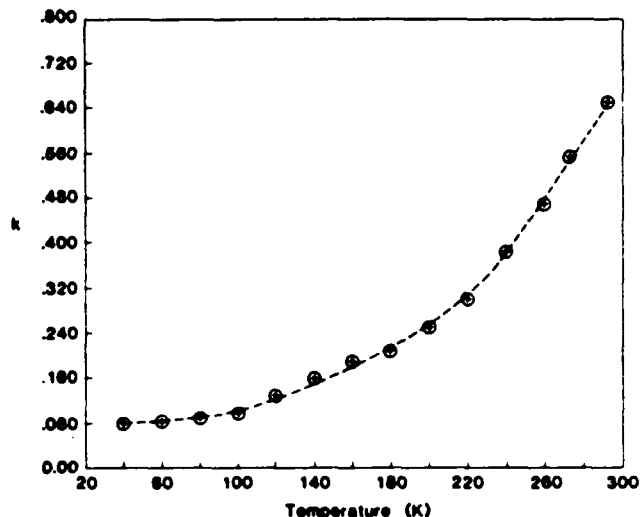Figure 4. Temperature dependence of n
            for BSKNN c-axis.

Figure 5. Temperature dependence of k
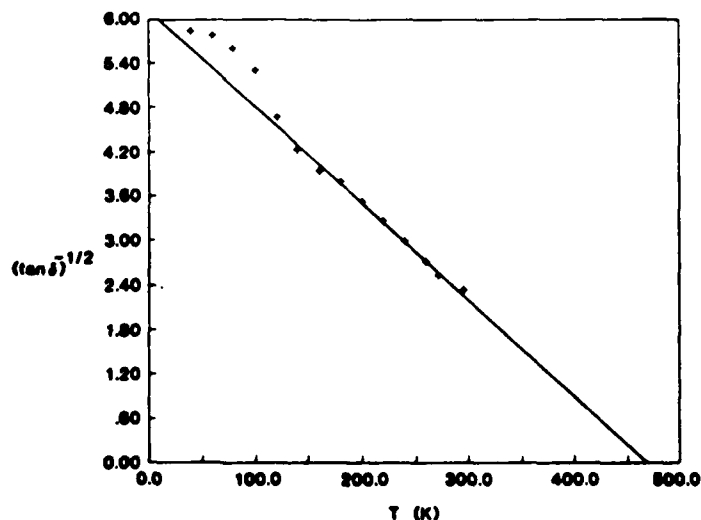   for BSKNN c-axis.

Figure 6. Temperature dependence of loss tangent
            to the -1/2 power for BSKNN c-axis.

2-4

Discussion

The decrease in absorption along the c-axis upon cooling is expected if the radiation is absorbed by the ferroelectric soft mode. This is an optic phonon mode with a resonant frequency which increases as the temperature decreases further away from the Curie temperature (476K for BSKNN). As the resonant frequency moves further away from millimeter wave frequencies, absorption decreases. A simple harmonic oscillator model for one-phonon absorption, together with a Curie-Weiss law for the phonon frequency, implies that the reciprocal of the loss tangent should vary linearly with temperature, intersecting the T axis at the Curie temperature.[11] Although this model does not fit the BSKNN data, the linear fit described is obtained if the loss tangent is replaced by its square root, as shown in Figure 6. Note that the intercept is indeed at the Curie temperature. The absorption mechanism leading to this behavior is not known and further evidence of the inadequacy of this soft mode model is evidenced by the frequency dependencies of n and k. Adjustment of soft mode parameters cannot produce a theoretical transmittance spectrum which fits the data as well as when n and k are constant over the spectrum.

It is noted that both of these crystals become millimeter wave polarizers at low temperatures, absorbing one radiation polarization much more strongly than the other. The mechanism for this behavior is not yet understood. This polarizing property is particularly interesting when one considers how rare are crystals, such as tourmaline or herapathite (used in Polaroid sheets), which polarize visible light by absorption.

To take advantage of the low losses in these cooled crystals, an electrooptic device should have the crystal axis parallel to the radiation polarization. This geometry has been shown to give the largest electrooptic effect for visible waves in SBN.[12] It seems likely that this also gives the largest effect for millimeter waves. The effect that has been measured in SBN[3] was actually a linear combination of effects along the c- and a-axes.

Conclusion

The millimeter wave absorption of two tungsten bronze ferroelectrics has been found to decrease dramatically for one orientataion upon cooling to cryogenic temperatures. This could greatly improve their performance as active elements in millimeter wave electrooptic devices. Low temperature measurements of their electrooptic coefficients are in progress to verify this assertion. Continued materials research on tungsten bronze ferroelectrics is also in progress to develop crystals which maximize the figure-of-merit[3] for use in electrooptic devices.

Acknowledgement

References
1. M.B. Klein, "Phase shifting at 94 GHz using the electrooptic effect in bulk crystals," Int. J. Infrared Millimeter Waves 2, 239 (1981).
2. M.B. Klein, "Dielectric waveguide modulators at 95 GHz using LiNbO$_3$," Int. J. Infrared Millimeter Waves 3, 587 (1982).
3. M.B. Klein, "Dielectric waveguide electrooptic devices," in Infrared and Millimeter Waves, v. 9 (K. Button, ed.), Academic Press, N.Y., 1983, pp. 123-175.
4. G.D. Boyd, T.J. Bridges, M.A. Pollack & E.H. Turner, "Microwave nonlinear susceptibilities due to electronic and ionic anharmonicities in acentric crystals," Phys. Rev. Lett. 26, 387 (1971).
5. W. Ho, W.F. Hall, R.R. Neurgaonkar, R.E. DeWames & T.C. Lim, "Microwave dielectric properties of SBN single crystals at 35 and 58 GHz," Ferroelectrics 38, 833 (1981).
6. R.R. Neurgaonkar, W.K. Cory, W.W. Ho, W.F. Hall & L.E. Cross, "Tungsten bronze family crystals for acoustical and dielectric application," Ferroelectrics 38, 857 (1981).
7. R.R. Neurgaonkar, W.K. Cory & J.R. Oliver, "Growth and applications of ferroelectric tungsten bronze family crystals," Southwest Conf. on Optics, Albuquerque (1985).
8. M. Matloubian, B. Bobbs, H.R. Fetterman & M.B. Klein, to be published.
9. J.A. How, P. Leuterer & M. Tutter, "A flexible waveguide for millimeter waves," Int. J. Infrared Millimeter Waves 4, 343 (1983).
10. W.B. Bridges, M.B. Klein & E. Schweig, "Measurement of the dielectric constant and loss tangent of thallium mixed halide crystals KRS-5 and KRS-6 at 95 GHz," IEEE Trans. MTT-30, 468 (1982).
11. M.E. Lines & A.M. Glass, Principles and Applications of Ferroelectrics and Related Materials, Clarendon Press, Oxford, 1977.
12. P.V. Lenzo, E.G. Spencer & A.A. Ballman, "Electrooptic coefficients of ferroelectric SBN," Appl. Phys. Lett. 11, 23 (1967).

Rockwell International
Science Center

... where science gets down to business

END

FILMED

9-85

DTIC